

# A hybrid moment method for multi-scale kinetic equations based on maximum entropy principle

Weiming Li<sup>\*</sup>, Peng Song<sup>†</sup>, Yanli Wang<sup>‡</sup>

April 14, 2020

## Abstract

We propose a hybrid moment method for the multi-scale kinetic equations in the framework of the regularized moment method [7]. In this method, the fourth order moment system is chosen as the governing equations in the fluid region. When transiting from the fluid regime to the kinetic regime, the maximum entropy principle is adopted to reconstruct the kinetic distribution function, so that the information in the fluid region can be utilized thoroughly. Moreover, only one uniform set of numerical scheme is needed for both the fluid and kinetic regions. Numerical tests show the high efficiency of this new hybrid method.

**Keywords:** hybrid method, regularized moment method, maximum entropy method, Boltzmann equation

## 1 Introduction

Traditional fluid models, such as Euler and the Navier-Stokes equations, give accurate descriptions of gas flows when the system is close to an equilibrium state. However, many problems, such as simulations of hypersonic flows, involve non-equilibrium processes, where traditional fluid models break down. In this case, the kinetic equations, such as the Boltzmann equation, are introduced to describe the evolution of the particles. However, due to its high dimensionality, the computational cost to simulate the kinetic equation is quite expensive in comparison to using fluid models such as Euler or Navier-Stokes equations.

Several parameters are introduced to describe how far the particles are from the equilibrium, for example the Knudsen number. The Knudsen number is defined as the ratio of the mean free path of the particles to a typical macroscopic length. When the Knudsen number is large, the flow is in the kinetic regime, and the simulations are studied by the kinetic equations, for example the Boltzmann equation. As to the Boltzmann equation, several kinds of numerical methods have been proposed. The DSMC (Direct Simulation Monte Carlo) method [3] is a stochastic numerical method, which is quite efficient when the Knudsen number is large, but may be expensive for the fluid regime. There are also several classical deterministic methods, for example discrete velocity method [19, 31], and the spectral method such as the Fourier spectral method [32, 29, 16]. Moreover, Hermite spectral method is also introduced to solve the Boltzmann equation [18, 38], which can be traced back to Grad's classical paper [20]. Despite the several kinds of numerical methods that have been proposed, the numerical cost of Boltzmann equations is still quite prohibitive due to the high dimensionality.

For the multi-scale problems, where the fluid and kinetic regions are both included, the coupling of the kinetic and fluid dynamic equations has become an important research area [26, 15, 14]. In [26], a moment realizability matrix is introduced to differentiate the fluid region and the kinetic region. Then the moment realizability matrix is utilized in [14, 15, 39] as a criterion for solving the multi-scale kinetic problems. There are several other hybrid methods, which are based on the local Knudsen number [24] or based on the viscosity and heat flux of the Navier-Stokes equations [36, 2]. Moreover, the hybridization of the Monte Carlo method and the finite volume method is proposed in [4, 10, 11].

Recently a globally hyperbolic moment method is proposed in [7, 5] to solve the Boltzmann equation. This method is based on a Hermite spectral method where the expansion center is chosen as the local

<sup>\*</sup>Laboratory of Computational Physics, Institute of Applied Physics and Computational Mathematics, Beijing, China, 100088, email: [liweiming@pku.edu.cn](mailto:liweiming@pku.edu.cn)

<sup>†</sup>Laboratory of Computational Physics, Institute of Applied Physics and Computational Mathematics, Beijing, China, 100088, email: [song-peng@iapcm.ac.cn](mailto:song-peng@iapcm.ac.cn)

<sup>‡</sup>Beijing Computational Science Research Center, Beijing, China, 100193, email: [ylwang@csrc.ac.cn](mailto:ylwang@csrc.ac.cn).

velocity and temperature, where it is expected that this expansion can describe the distribution function well even when it is far from the equilibrium. A highly efficient numerical scheme has been designed under the framework of this method, which also has been successfully used to solve Vlasov and Wigner equations [22]. It is also proved that the moment system derived by the hyperbolic moment method contains the fluid dynamic equations such as Euler and Navier-Stokes equations. This method is verified to successfully simulate the movement of the particles with any Knudsen number. But the expansion order may increase quickly with the increase of the Knudsen number. Therefore, when there is a coupling of kinetic and fluid regimes, for example in the simulations of the hypersonic flows around a space vehicle during the re-entry phase, there may exist large variation of the Knudsen number, in which case, the expansion order is decided by the largest Knudsen number, and the computational cost may be expensive.

In this paper, we propose a uniform hybrid method in the framework of the regularized moment method [7]. Instead of Euler and the Navier-Stokes equations, the moment equations with expansion order four are utilized as the governing equations in the fluid region. The reason that we choose the fourth order moment model as our fluid model is that the maximum entropy ansatz for reconstructing the kinetic distribution function is utilized when we change from fluid to kinetic description, and the fourth order system is the smallest moment system in the maximum entropy theory where the distribution ansatz could characterize non-equilibrium behavior. Another important point of the hybrid method is the domain decomposition indicator. In our hybrid method, the domain decomposition indicator is based on the moment realizability matrices proposed in [26] and later used in [14, 15]. It has quite a simple form, where instead of the derivatives of the macroscopic variables, only the expansion coefficients of the distribution function with orders smaller than four are used. The criteria from/to hydrodynamic to/from kinetic are proposed based on the indicator. Numerical tests show that our method could describe the evolution of the particles in the fluid region with quite few degrees of freedom and is therefore more efficient than the traditional regularized moment method using a uniform number of moments. Another advantage of our method is that we could use same numerical scheme for both the kinetic and fluid regions. We do not need to strictly discriminate the numerical flux in different domains, especially those at the kinetic and fluid interfaces, since they all have the same form, which simplifies the coupling of different domains. Numerical simulations are done for several benchmark problems. In the numerical test, the BGK and Shakhov collision term are applied, with the dimension reduction method in the microscopic velocity space in [6] adopted to reduce computation complexity.

The rest of this paper is organized as follows: Section 2 introduces the Boltzmann equation, and two moment methods including the maximum entropy method [25] and the regularized moment methods [7] briefly. The detailed hybrid method is given in Section 3, and the numerical algorithm is also proposed in this section. Several numerical examples are exhibited in Section 4. Conclusion and future work are made in Section 5. Detailed description of the numerical scheme and the method to solve the maximum entropy method is given in the Appendix.

## 2 Boltzmann equation and the moment method

In the kinetic theory, the Boltzmann equation is always adopted to describe the movement of the particles, especially in the rarefied gas dynamics. However, when the gas becomes dense, in other words when the system approaches the fluid regime, the Boltzmann equation may reduce to Euler or Navier-Stokes equations. In this section, we will first introduce the Boltzmann equation [34] and some related properties.

### 2.1 Boltzmann equation

In the Boltzmann equation, the distribution function  $f(t, \mathbf{x}, \mathbf{v})$  is used to describe the fluid state, where  $t$  is time,  $\mathbf{x}$  is the spatial space, and  $\mathbf{v}$  stands for the velocity of gas molecules. The dimensionless form of the governing equation is

$$\frac{\partial f}{\partial t} + \mathbf{v} \cdot \nabla_{\mathbf{x}} f = \frac{1}{\epsilon} \mathcal{Q}[f], \quad t \in \mathbb{R}^+, \quad \mathbf{x} \in \mathbb{R}^3, \quad \mathbf{v} \in \mathbb{R}^3, \quad (2.1)$$

where  $\epsilon$  is a formal smallness parameter which plays the role of Knudsen number.  $\mathcal{Q}[f]$  denotes particle collision, which may have quite complex form. The collision operator satisfies the following properties:

1. conservation of the mass, momentum and kinetic energy

$$\int_{\mathbb{R}^3} \begin{pmatrix} 1 \\ \mathbf{v} \\ |\mathbf{v}|^2 \end{pmatrix} \mathcal{Q}[f] d\mathbf{v} = 0. \quad (2.2)$$

2. the Boltzmann's H-theorem

$$\int_{\mathbb{R}^3} \mathcal{Q}[f] \log f \, d\mathbf{v} \leq 0, \quad (2.3)$$

where equality holds if and only if  $f$  is the Maxwellian, which is the steady state of the Boltzmann equation (2.1)

$$\mathcal{M} = \frac{\rho}{(2\pi\theta)^{3/2}} \exp\left(-\frac{|\mathbf{v} - \mathbf{u}|^2}{2\theta}\right). \quad (2.4)$$

Here  $\rho(t, \mathbf{x})$  is the density,  $\mathbf{u}(t, \mathbf{x})$  is the macroscopic velocity and  $\theta(t, \mathbf{x})$  is the temperature of the particles, whose relationships with the distribution function  $f(t, \mathbf{x}, \mathbf{v})$  is as below

$$\begin{pmatrix} \rho(t, \mathbf{x}) \\ \rho(t, \mathbf{x})\mathbf{u}(t, \mathbf{x}) \\ \frac{1}{2}\rho|\mathbf{u}(t, \mathbf{x})|^2 + \frac{3}{2}\rho(t, \mathbf{x})\theta(t, \mathbf{x}) \end{pmatrix} = \int_{\mathbb{R}^3} \begin{pmatrix} 1 \\ \mathbf{v} \\ \frac{1}{2}|\mathbf{v}|^2 \end{pmatrix} f(t, \mathbf{x}, \mathbf{v}) \, d\mathbf{v}. \quad (2.5)$$

Moreover, it also holds that

$$\mathcal{Q}(\mathcal{M}) = 0. \quad (2.6)$$

3. Galilean invariance:  $\mathcal{Q}[f]$  commutes with translational and rotational operators.

In this paper, we are mainly concerned with the hybrid method to solve the Boltzmann equation, therefore, the simplified collision operator is used here, for example the BGK collision operator

$$\mathcal{Q}^{\text{BGK}}[f] = \frac{1}{\tau}(\mathcal{M} - f), \quad (2.7)$$

where  $\tau$  is the relaxation time, which is usually obtained from the first approximation of the Chapman-Enskog theory [3].  $\tau$  is a parameter that related to the Knudsen number  $Kn$  and some macroscopic variables such as the density. When  $\tau$  is large, very few molecular collisions occur, and the entire flow is rarefied. For the classical BGK operator, it gives the wrong Prandtl number which equals 1 whereas the correct Prandtl number for a monoatomic gas is  $2/3$ . Another simplified collision operator, the Shakhov collisional operator preserves the correct Prandtl number [34], which has the form

$$\mathcal{Q}_{\text{Shakhov}}(f) = \frac{1}{\tau}(f_s - f), \quad f_s = P_3(t, \mathbf{x}, \mathbf{v})\mathcal{M}(t, \mathbf{x}, \mathbf{v}), \quad (2.8)$$

with

$$P_3 = 1 + \frac{(1 - \text{Pr})(\mathbf{v} - \mathbf{u}) \cdot \mathbf{q}}{(D + 2)\rho(t, \mathbf{x})[\theta(t, \mathbf{x})]^2} \left( \frac{|\mathbf{v} - \mathbf{u}|^2}{\theta(t, \mathbf{x})} - (D + 2) \right), \quad D = 3, \quad (2.9)$$

where  $D$  is the dimension number of the microscopic velocity space and  $\text{Pr}$  is the Prandtl number.  $\mathbf{q}$  is heat flux, which is defined as

$$q_i = \frac{1}{2} \int_{\mathbb{R}^3} |\mathbf{v} - \mathbf{u}|^2 (v_i - u_i) f \, d\mathbf{v}, \quad i = 1, 2, 3. \quad (2.10)$$

There are other physical variables people are interested in, such as the stress tensor  $\sigma_{ij}$ , which is defined as

$$\sigma_{ij} = \int_{\mathbb{R}^3} \left( (v_i - u_i)(v_j - u_j) - \frac{1}{3}\delta_{ij}|\mathbf{v} - \mathbf{u}|^2 \right) f \, d\mathbf{v}, \quad i, j = 1, 2, 3. \quad (2.11)$$

Besides, the pressure tensor  $p_{ij}$  is defined as

$$p_{ij} = \int_{\mathbb{R}^3} (v_i - u_i)(v_j - u_j) f \, d\mathbf{v}, \quad \sigma_{ij} = p_{ij} - \frac{1}{3}\delta_{ij} \sum_{k=1}^3 p_{kk}. \quad (2.12)$$

*Remark 1.* In our numerical test, we choose the VHS model for  $\tau$  as

$$\tau = \sqrt{\frac{\pi}{2}} \frac{15Kn}{(5 - 2\omega)(7 - 2\omega)} \frac{\theta^{\omega-1}}{\rho}, \quad (2.13)$$

where  $\omega$  is the viscous index dependent on the type of the particles, and  $Kn$  is the Knudsen number. Moreover,  $\tau$  is also the same parameter to indicate the regime of the particles in some literature [14, 15].

There has been much active research on algorithms for solving the Boltzmann equation numerically, especially for problems in the transitional regime, such as [13, 17, 35, 7]. In this paper, we focus on developing a hybrid moment method under the framework of the globally hyperbolic moment method [7, 5], with a strategy that utilizes the closure method based on the maximum entropy principle [25, 21, 27]. In the next section, we will briefly introduce these two methods.

## 2.2 Maximum entropy moment method

For simplicity and without loss of generality, this section considers the 1D case in microscopic velocity space. Define the  $k$ -th order moment as

$$\mu_k = \langle f \rangle_k = \int_{\mathbb{R}} f v^k dv. \quad (2.14)$$

We could obtain the time evolution equation of  $\mu_k$  by multiplying Equation (2.1) by  $v^k$  and integrating against  $v$  over  $\mathbb{R}$ :

$$\frac{\partial \mu_k}{\partial t} + \frac{\partial \mu_{k+1}}{\partial x} = \left\langle \frac{1}{\epsilon} \mathcal{Q}[f] \right\rangle_k, \quad k \in \mathbb{N}. \quad (2.15)$$

Because in Equation (2.15), the governing equation of  $\mu_k$  depends on  $\mu_{k+1}$ , therefore the full system contains an infinite number of equations. We do a truncation in order to obtain a reduced model for Equation (2.1). Specifically, we choose a fixed integer  $M$  and discard all equations for  $\mu_k$ ,  $k > M$ . Still, as the truncated moment system depends on  $\mu_{M+1}$ , it is not a closed system, so a *moment closure* is needed in the system. One way of specifying a closure is to construct an ansatz for the distribution function. Specifically, given moments  $\mu_k$ ,  $k = 0, \dots, M$ , one could reconstruct an ansatz of the distribution function,  $\hat{f}$ , which satisfies

$$\langle \hat{f}(v; \mu_0, \dots, \mu_M) \rangle_k = \mu_k, \quad k = 0, \dots, M. \quad (2.16)$$

Then the moment closure could be given by

$$\mu_{M+1} = \langle \hat{f}(v; \mu_0, \dots, \mu_M) \rangle_{M+1}. \quad (2.17)$$

The maximum entropy moment method closes the system (2.15) by specifying an ansatz of  $f$  based on the entropy minimization principle [12, 23, 25, 30]. Specifically, the ansatz  $\hat{f}$  finds the most likely distribution function under constraints of the given moments by solving the following functional minimization problem

$$\hat{f} = \operatorname{argmin} H(f), \quad \text{s.t.} \langle \hat{f}(v) \rangle_k = \mu_k, \quad k = 0, \dots, M, \quad (2.18)$$

with  $H(f) = \langle f \log f - f \rangle$ . Direct computation shows the unique solution of Equation (2.18) has the form

$$\hat{f} = \exp \left( \sum_{k=0}^M \lambda_k v^k \right), \quad (2.19)$$

where  $\lambda_k$ ,  $k = 0, \dots, M$  are called the Lagrange multipliers. Since Equation (2.19) is in the integrable function space, the highest order of the polynomial  $\sum_{k=0}^M \lambda_k v^k$  should be even.

The simplest model in the maximum entropy hierarchy that contains all the conserved variables is the Euler equation. It is sufficient for the description of processes in local thermodynamic equilibrium, but even in moderately rarefied gas flows, stronger deviations from equilibrium may be expected, making the closing relationship of Euler equation unsound. The next model in the maximum entropy hierarchy is the fourth order moment model, which extends the validity of the Euler system by including some higher order moments such as the heat flux. Levermore [25] proved that the maximum entropy moment model has many nice properties, the most important of which are that it is globally hyperbolic, dissipates the physical entropy, and that it always corresponds to a non-negative ansatz. Unfortunately, for the maximum entropy moment hierarchy, if moments beyond the second order are included, no closed-form expressions for the closing relationships are available. This entails solving an optimization problem which is usually computationally expensive [1, 28, 33].

On the other hand, the regularized moment method is another approach to obtain hyperbolic closures for a hierarchy of moment system. However, for the regularized moment method, closed-form expressions for closing fluxes are always available, making simulation with the regularized moment method much more efficient for high order moment systems. We will briefly review the regularized moment method in the next section.

## 2.3 The regularized moment method

The globally hyperbolic regularized moment method was first proposed in [7] to solve the Boltzmann equations, which is also validated to be efficient to solve the Wigner, Vlasov equations [22], and also

applied to the radiative transfer problems. Under the framework of the regularized moment method, the distribution function  $f$  is approximated by series expansion of the basis functions and a special regularization is adopted to the globally hyperbolic moment systems. Precisely, the distribution function  $f(t, \mathbf{x}, \mathbf{v})$  is expanded as

$$f(t, \mathbf{x}, \mathbf{v}) = \sum_{\alpha \in \mathbb{N}^3} f_\alpha(t, \mathbf{x}) \mathcal{H}_\alpha^{\mathbf{u}, \theta}(\mathbf{v}), \quad (2.20)$$

where  $\alpha = (\alpha_1, \alpha_2, \alpha_3)$  is a three-dimensional multi-index, and the basis functions  $\mathcal{H}_\alpha^{\mathbf{u}, \theta}(\mathbf{v})$  are defined as

$$\mathcal{H}_\alpha^{\mathbf{u}, \theta}(\mathbf{v}) = \prod_{i=1}^3 \frac{1}{\sqrt{2\pi}} \theta^{-\frac{\alpha_i+1}{2}} He_{\alpha_i}(\xi_i) \exp\left(-\frac{\xi_i^2}{2}\right), \quad \xi_i = \frac{v_i - u_i}{\sqrt{\theta}}, \quad (2.21)$$

where  $He_{\alpha_i}$  is the Hermite polynomial. Under this expansion, the relationship between the moment coefficients  $f_\alpha$  and the macroscopic variables are as below

$$\begin{aligned} f_0 &= \rho(t, \mathbf{x}), \quad f_{e_i} = 0, \quad \sum_{j=1}^3 f_{2e_j} = 0, \\ q_i &= 2f_{3e_i} + \sum_{d=1}^3 f_{2e_d+e_i}, \quad \sigma_{ij} = (1 + \delta_{ij})f_{e_i+e_j}, \quad i, j = 1, 2, 3. \end{aligned} \quad (2.22)$$

With this expansion, the Maxwellian (2.4) can be expressed by only the zeroth-order of expansion as

$$\mathcal{M} = f_0(t, \mathbf{x}) \mathcal{H}_0^{\mathbf{u}, \theta}(\mathbf{v}), \quad f_0 = \rho. \quad (2.23)$$

With a truncation of (2.20), we can get a finite approximation of the distribution function. Precisely, we let  $M \geq 3$  be a positive number and only the coefficients in the set  $\mathcal{S} = \{f_\alpha\}_{|\alpha| \leq M}$  are considered. Thus, the expansion is truncated as

$$f(t, \mathbf{x}, \mathbf{v}) \approx \sum_{|\alpha| \leq M} f_\alpha(t, \mathbf{x}) \mathcal{H}_\alpha^{\mathbf{u}, \theta}(\mathbf{v}). \quad (2.24)$$

Following the procedure in [7], we can get the globally hyperbolic moment systems. Precisely, substituting the expansion (2.21) into the Boltzmann equation (2.1) and adopting the regularization in [7], we can get the globally hyperbolic moment equations (HME) for the Boltzmann equation,

$$\begin{aligned} \frac{\partial f_\alpha}{\partial t} + \sum_{j=1}^D \left( \theta \frac{\partial f_{\alpha-e_j}}{\partial x_j} + u_j \frac{\partial f_\alpha}{\partial x_j} + (1 - \delta_{M, |\alpha|})(\alpha_j + 1) \frac{\partial f_{\alpha+e_j}}{\partial x_j} \right) + \sum_{d=1}^D \frac{\partial u_d}{\partial t} f_{\alpha-e_d} \\ + \sum_{j,d=1}^D \frac{\partial u_d}{\partial x_j} (\theta f_{\alpha-e_d-e_j} + u_j f_{\alpha-e_d} + (1 - \delta_{M, |\alpha|})(\alpha_j + 1) f_{\alpha-e_d+e_j}) + \frac{1}{2} \frac{\partial \theta}{\partial t} \sum_{d=1}^D f_{\alpha-2e_d} \\ + \sum_{j,d=1}^D \frac{1}{2} \theta \frac{\partial \theta}{\partial x_j} (\theta f_{\alpha-2e_d-e_j} + u_j f_{\alpha-2e_d} + (1 - \delta_{M, |\alpha|})(\alpha_j + 1) f_{\alpha-2e_d+e_j}) = Q_\alpha, \quad |\alpha| \leq M, \end{aligned} \quad (2.25)$$

where  $\delta$  is the Kronecker's delta, and  $f_\alpha$  is taken as zero if any component of  $\alpha$  is negative.  $Q_\alpha$  is the expansion of the collision term. If we take the BGK collision model (2.7), then

$$Q_\alpha^{\text{BGK}} = \begin{cases} -\frac{1}{\tau} f_\alpha, & |\alpha| \geq 2, \\ 0, & \text{otherwise.} \end{cases} \quad (2.26)$$

For the Shakhov collision model, the collision coefficients  $Q_\alpha$  have the form as

$$Q_\alpha^{\text{shakhov}} = \begin{cases} \frac{1}{\tau} \left( \frac{1-Pr}{5} q_j - f_\alpha \right), & \alpha = 2e_i + e_j, \quad i, j = 1, 2, 3, \\ Q_\alpha^{\text{BGK}}, & \text{otherwise.} \end{cases} \quad (2.27)$$

Collecting all the independent variables of  $f_\alpha$ ,  $\mathbf{u}$  and  $\theta$  as a vector  $\mathbf{w}$ , then the system (2.25) can be written in a quasi-linear form

$$\mathbf{D}(\mathbf{w}) \frac{\partial \mathbf{w}}{\partial t} + \sum_{j=1}^D \mathbf{M}_j(\mathbf{w}) \mathbf{D}(\mathbf{w}) \frac{\partial \mathbf{w}}{\partial x_j} = \mathbf{g}(\mathbf{w}), \quad (2.28)$$

where  $\mathbf{D}\frac{\partial \mathbf{w}}{\partial t}$  corresponds to the time derivative in (2.25) while  $\mathbf{M}_j \mathbf{D}\frac{\partial \mathbf{w}}{\partial x_j}$  describes the convection term on the  $x_j$  direction, and  $\mathbf{g}$  denotes the right hand side of (2.25). The detailed expression can be found in [6], and the form is put here only for the sake of convenience. In [5, 37], the moment system (2.28) is proved to be globally hyperbolic and a highly efficient numerical scheme is designed in the framework of the regularized moment method, where the general finite volume method is used in the spatial space. The detailed numerical scheme is introduced in the Appendix A.

For the rarefied gas, especially when the Knudsen number is large, quite a large expansion number  $M$  is needed to approximate the distribution function. In the framework of the regularized moment method, the expansion number of the distribution function  $M$  is decided according to the largest Knudsen number, which may be quite expensive for the problems with large variation of the Knudsen number. It is still a large waste for the area where the Knudsen number is small. Therefore, the hybrid kinetic/fluid scheme in the framework of the regularized moment method is proposed in this paper to reduce the computational cost, with an indicator designed to adjust the expansion number according to the Knudsen number.

### 3 Hybrid regularized moment method

Many engineering problems involve both the fluid regime and the kinetic region. For the fluid regimes, the Euler or Navier-Stokes like fluid description is enough to solve the problem. However, for the kinetic region, we should use the kinetic model to accurately describe the system. The kinetic model is always quite expensive to solve, even in the framework of the regularized moment method. Therefore, for the sake of computational efficiency, several so-called hybrid kinetic/fluid schemes are proposed [15, 14] with an automatic domain-decomposition criterion. In this section, we will also introduce a hybrid method in detail.

#### 3.1 Regime indicator and criterion

In this section, the indicator matrix for the hybrid moment method and the specific criterion is proposed. We will start from the analysis of the moment system (2.25) derived in the regularized moment method. Following the method in [7], we can deduce the equations of density, velocity and temperature when setting  $\alpha = 0$ ,  $e_i$  and  $2e_i$  respectively as

$$\begin{aligned} \frac{\partial \rho}{\partial t} + \sum_{j=1}^3 \left( u_j \frac{\partial \rho}{\partial x_j} + \rho \frac{\partial u_j}{\partial x_j} \right) &= 0, \\ \rho \left( \frac{\partial u_d}{\partial t} + \sum_{j=1}^3 u_j \frac{\partial u_d}{\partial x_j} \right) + \sum_{j=1}^3 \frac{\partial p_{jd}}{\partial x_j} &= 0, \quad d = 1, 2, 3, \\ \rho \left( \frac{\partial \theta}{\partial t} + \sum_{j=1}^3 u_j \frac{\partial \theta}{\partial x_j} \right) + \frac{2}{3} \sum_{j=1}^3 \left( \frac{\partial q_j}{\partial x_j} + \sum_{d=1}^3 p_{jd} \frac{\partial u_d}{\partial x_j} \right) &= 0. \end{aligned} \quad (3.1)$$

When the distribution function  $f$  is Maxwellian (2.4), the stress tensor and heat flux are reduced into

$$p_{ij} = \delta_{ij} \rho \theta, \quad q_i = 0, \quad i, j = 1, 2, 3. \quad (3.2)$$

Then with some rearrangement, we can find that the moment system (3.1) is reduced into the Euler equations

$$\begin{cases} \frac{\partial \rho}{\partial t} + \nabla_{\mathbf{x}} \cdot (\rho \mathbf{u}) = 0, \\ \frac{\partial (\rho \mathbf{u})}{\partial t} + \nabla_{\mathbf{x}} \cdot (\rho \mathbf{u} \otimes \mathbf{u} + \rho \theta \mathbf{I}) = \mathbf{0}, \\ \frac{\partial E}{\partial t} + \nabla_{\mathbf{x}} \cdot (\mathbf{u}(E + \rho \theta)) = 0, \end{cases} \quad (3.3)$$

where  $E = \frac{1}{2}\rho|\mathbf{u}|^2 + \frac{3}{2}\rho\theta$  is the kinetic energy. Similarly, we can also get the Navier-Stokes equation from (3.1)

$$\begin{cases} \frac{\partial \rho}{\partial t} + \nabla_{\mathbf{x}} \cdot (\rho \mathbf{u}) = 0, \\ \frac{\partial(\rho \mathbf{u})}{\partial t} + \nabla_{\mathbf{x}} \cdot (\rho \mathbf{u} \otimes \mathbf{u} + \rho \theta \mathbf{I}) = \nabla_{\mathbf{x}} \cdot \boldsymbol{\sigma}, \\ \frac{\partial E}{\partial t} + \nabla_{\mathbf{x}} \cdot (\mathbf{u}(E + \rho \theta)) = \nabla_{\mathbf{x}} \cdot (\boldsymbol{\sigma} \cdot \mathbf{u} + \mathbf{q}), \end{cases} \quad (3.4)$$

where the relationship between  $\boldsymbol{\sigma}, \mathbf{q}$  and  $\mathbf{u}, \theta$  will be given by some kind of Fourier law [34], which will lead to a closed equation system. From the analysis above, we can see that Euler and Navier-Stokes equations are included in the moment equations (2.25). With the same procedure, we can find that the high order equations similar to Burnett and Super-Burnett equations can also be deduced. With the increase of the extension number, the moment equations are also validated to describe the movements of the particles in the rarefied gas problems.

Those macroscopic equations can also be deduced from the Chapman-Enskog expansion of the distribution functions, where the distribution function is expanded as

$$f = \mathcal{M} \left[ 1 + \epsilon g^{(1)} + \epsilon^2 g^{(2)} + \dots \right], \quad (3.5)$$

with  $g^{(i)}$  the fluctuations which depend on  $\rho, \mathbf{u}, \theta$  and their finite derivatives. The Euler equation could be derived by assuming a zeroth order expansion with respect to  $\epsilon$ , in other words,  $\hat{f} = \mathcal{M}$ . The first order expansion with respect to  $\epsilon$  would yield Navier-Stokes equations, while higher order expansions corresponds to Burnett and super-Burnett equations.

Then we will introduce the indicator matrix for the moment equations, which could distinguish the fluid region and the kinetic region. We will first introduce the two variables

$$\mathbf{A}(\mathbf{v}) = \int_{\mathbb{R}^3} \left( \boldsymbol{\xi} \otimes \boldsymbol{\xi} - \frac{|\boldsymbol{\xi}|^2}{3} \mathbf{I} \right) f(t, \mathbf{x}, \mathbf{v}) d\mathbf{v}, \quad \mathbf{B}(\boldsymbol{\xi}) = \int_{\mathbb{R}^3} \frac{1}{2} (|\boldsymbol{\xi}|^2 - 5) \boldsymbol{\xi} f(t, \mathbf{x}, \mathbf{v}) d\mathbf{v}, \quad \boldsymbol{\xi} = \frac{\mathbf{v} - \mathbf{u}}{\sqrt{\theta}}. \quad (3.6)$$

If the distribution function  $f$  is reduced into Maxwellian, we can get the Euler equations. In this case, it holds that

$$\int_{\mathbb{R}^3} \mathbf{A} f d\mathbf{v} = \int_{\mathbb{R}^3} \mathbf{B} f d\mathbf{v} = 0. \quad (3.7)$$

If  $f \approx \mathcal{M}(1 + \epsilon g^{(1)})$ , then we can deduce Navier-Stokes equations, in which case,

$$\int_{\mathbb{R}^3} \mathbf{A} f d\mathbf{v} \neq 0, \quad \int_{\mathbb{R}^3} \mathbf{B} f d\mathbf{v} \neq 0. \quad (3.8)$$

If the distribution function  $f$  has the form (3.5), (3.8) still holds. Thus, it is natural to use  $\mathbf{A}$  and  $\mathbf{B}$  to get the regime indicators in order to discriminate the particle regimes. Actually, it has already been successfully used in several works to detect the fluid regions, such as [14, 15], where a moment realizability matrix is proposed based on  $\mathbf{A}$  and  $\mathbf{B}$  to describe the domain decomposition criteria as

$$\mathbf{M} := \mathbf{m} \otimes \mathbf{m} \quad \mathbf{m} = \left( 1, \boldsymbol{\xi}, \sqrt{\frac{2}{3}} \left( \frac{|\boldsymbol{\xi}|^2}{2} - \frac{3}{2} \right) \right), \quad \boldsymbol{\xi} = \frac{\mathbf{v} - \mathbf{u}}{\sqrt{\theta}}. \quad (3.9)$$

In the framework of the regularized moment method, we can find that the corresponding coefficient matrix of the moment realizability matrix (3.9) is

$$\mathbf{I} = \frac{1}{\rho} \int_{\mathbb{R}^3} \mathbf{M} f(t, \mathbf{x}, \mathbf{v}) d\mathbf{v} = \begin{pmatrix} 1 & 0 & 0 & 0 & 0 \\ 0 & \frac{p_{11}}{\rho\theta} & 0 & 0 & \frac{\sqrt{2}q_1}{\sqrt{3\rho\theta^{3/2}}} \\ 0 & 0 & \frac{p_{22}}{\rho\theta} & 0 & \frac{\sqrt{2}q_2}{\sqrt{3\rho\theta^{3/2}}} \\ 0 & 0 & 0 & \frac{p_{33}}{\rho\theta} & \frac{\sqrt{2}q_3}{\sqrt{3\rho\theta^{3/2}}} \\ 0 & \frac{\sqrt{2}q_1}{\sqrt{3\rho\theta^{3/2}}} & \frac{\sqrt{2}q_2}{\sqrt{3\rho\theta^{3/2}}} & \frac{\sqrt{2}q_3}{\sqrt{3\rho\theta^{3/2}}} & C \end{pmatrix}, \quad (3.10)$$

where

$$C = \frac{1}{\rho} \int_{\mathbb{R}^3} \frac{2}{3} \left( \frac{|\boldsymbol{\xi}|^2}{2} - \frac{3}{2} \right)^2 f(t, \mathbf{x}, \mathbf{v}) d\mathbf{v} = \frac{4}{\rho\theta^2} \sum_{j=1}^3 f_{4e_k} + \frac{2}{3\rho\theta^2} \sum_{i,j=1}^3 (1 - \delta_{ij}) f_{2e_i+2e_j} + 1. \quad (3.11)$$

For the moment, we have introduced the moment realizability matrix made of the expansion coefficients of the distribution function. Then we will introduce the criteria of the hybrid method. Before that, the governing equation in the fluid regime is proposed first.

From the moment systems (2.25), we can find that the moment systems contain Euler and Navier-Stokes equations. However, instead of the Euler and Navier-Stokes equations, the fourth order moment system is utilized in the fluid region. Our reason for choosing a fourth-order moment system on the macroscopic subdomains is as follows: for the fluid regime, we hope our method could cover the Navier-Stokes limit as it has wider applications than the Euler equation. At the same time, noting that if we need to switch from the fluid regime to the kinetic regime, we would need to specify an ansatz of the distribution function from the few moments which are all the information of the solution on the fluid subdomain to determine the data for the kinetic subdomain. We wish to use the maximum entropy distribution function to recover the kinetic distribution, as it is the most likely distribution function corresponding to the limited given information. The lowest order system in the maximum entropy model hierarchy which includes the Navier-Stokes limit is the fourth-order moment model, which has a similar hyperbolic form as the fourth-order moment model in the regularized moment hierarchy, with only the closure being different. Therefore, choosing the fourth-order moment model as the model used in the fluid regime allows us to not only retain the wide applicability of the Navier-Stokes equation, but also maintain the accuracy of the distribution function provided by the maximum entropy principle when the regime is changing from fluid to kinetic.

As a result, we propose a coupling procedure between a fourth-order moment system and an arbitrarily high order moment system under the framework of the regularized moment method. For the Euler equations, we can find that the matrix (3.10) is reduced into the Identity matrix. When the moment number equals four, we can get the same number of the moment coefficients least demanded by the maximum entropy method in 2.2. Moreover, the indicator matrix will remain the same for any expansion number larger than four. Therefore, the specific criteria and the closure method from the fluid region to kinetic region are proposed based on the moment realizability matrix (3.9) and the maximum entropy method.

**From kinetic to fluid** Supposing the eigenvalues of (3.10) other than 1 are  $\lambda_i, i = 1, 2, 3$ . We will first propose the criterion from the kinetic region to the fluid region. There exist a large number of methods [15, 14, 26, 24, 4] to decide how far the gas is from the equilibrium. Here, we adopt the simple comparison between the eigenvalues  $\lambda_i$  and 1. The detailed criterion is then as follows: The kinetic description could be reduced into the fluid description if the two conditions below are satisfied.

1. the eigenvalues are all close to the eigenvalues of the Euler equations which all equal 1.

$$\max_{i=1,2,3} |\lambda_i - 1| \leq \epsilon_1. \quad (3.12)$$

2. the  $l_1$  norm of the expansion coefficients of the distribution function  $f_\alpha$  when  $|\alpha| > 4$  is small.

$$\sum_{4 < |\alpha| \leq M} |f_\alpha| \leq \epsilon_2. \quad (3.13)$$

If both criteria are satisfied, the expansion number of the distribution function is set as  $M = 4$ . Then the region is changed from kinetic to fluid regime.

*Remark 2.* The two parameters  $\epsilon_1$  and  $\epsilon_2$  are problem-dependent. In our examples, they are set as  $\epsilon_1 = 10^{-3}$  and  $\epsilon_2 = 10^{-4}$ .

**From fluid to kinetic** The criterion from fluid region to kinetic region is similar, where the eigenvalues  $\lambda_i$  are also utilized. The detailed criterion is then as follows: The fluid description should be recovered to kinetic description if the condition below is satisfied.

1. at least one of the eigenvalues is far from the eigenvalues of the Euler equations.

$$\max_{i=1,2,3} |\lambda_i - 1| > \epsilon_1. \quad (3.14)$$

If the criterion is satisfied, the regime should be changed from the fluid region to the kinetic region. The expansion number of the distribution function is then reset to the maximum expansion number.

The only point left here is how to set the expansion coefficients of the distribution function when  $\alpha > 4$ . The easiest way is just to set them to zero. However, the fact that we need to reset the expansion number implies that the low order expansion and also setting the high order coefficients to zero may not be accurate enough to characterize the distribution function. Therefore, in this hybrid method, the maximum entropy method is applied here to derive the high order coefficients. This is also one of the reasons that we choose the fourth-order moment system instead of the Euler or Navier-Stokes equations in the fluid region.

In the maximum entropy method, we need to first recover a kinetic distribution function from the low order moments, which is all the information we have in the fluid regime. We do this by numerically solving the optimization problem Equation (2.18) where the known moments in the fluid regime (the first four order moments) are the given constraints. Then the recovered kinetic distribution function can be computed easily, based on which we can get the high order expansion coefficients. The algorithm to solve the specific optimization problem Equation (2.18) where the constraints are exactly the first four order moments is part of the subject of another paper in preparation, and some details are listed in Appendix B for the completeness. Due to the extreme complexity of solving the maximum entropy optimization problem, our current fast algorithm for solving the maximum entropy distribution function is constrained to 1D problems. In our numerical examples, the recovering of the maximum entropy distribution function from known moments is done for the dimension reduced distribution function.

For now, we have introduced the criterion to distinguish different regimes. In the next section, the detailed numerical scheme will be proposed, which is applied under the framework of the regularized moment with some adjustment in the interface between the fluid and kinetic regime.

### 3.2 Numerical Schemes

In the regularized moment method, the standard finite volume discretization is adopted in the spatial space. Firstly, the standard splitting method is applied, where the moment equations are split into the convection part and the collision part. The collision part is the same as that in the regularized moment method and we refer [7] for more details. For the convection part, the difference is the case that the expansion numbers are different in the adjacent cells. Here, we take the 1D spatial space as an example. Suppose  $\Gamma_h$  to be a uniform mesh in  $\mathbb{R}$ , and each cell is identified by an index  $j$ . For a fixed  $x_0 \in \mathbb{R}$  and  $\Delta x > 0$ , and the numerical solution to approximate the distribution function  $f$  at  $t = t_n$  is denoted as

$$f_h(x, \mathbf{v}) = f_j^n(\mathbf{v}) = \sum_{|\alpha| \leq M_j^n} f_{\alpha,j}^n \mathcal{H}_{\alpha}^{u_{1,j}^n, \theta_j^n}(\mathbf{v}), \quad x \in \Gamma_j, \quad (3.15)$$

where  $M_j^n$  is the expansion number at cell  $j$  and time  $t = t_n$  with  $u_{1,j}^n$  the first entry of  $\mathbf{u}_j^n$ . Assuming the expansion number on the cell  $j + 1$  are  $M_{j+1}^n$ . If  $M_{j+1}^n$  equals  $M_j^n$ , then the same HLL flux in [7] is utilized here. However, if they are different, we just take the algorithm below

1. Let  $M_j = \max(M_{j+1}^n, M_j^n)$ ;
2. Change the expansion number of  $f_{j+1}^n$  and  $f_j^n$  to  $M_j$ , where the increased expansion coefficients are set as 0. The reset distribution functions are labeled as  $f_j^{n,*}$  and  $f_{j+1}^{n,*}$ ;
3. Calculate the numerical flux  $F_{j+1/2}^{n,*}$  using HLL scheme with  $f_j^{n,*}$  and  $f_{j+1}^{n,*}$ ;
4. For the  $j$ -th cell, derive the numerical flux  $F_{j+1/2}^n$  by setting the expansion number of  $F_{j+1/2}^{n,*}$  as  $M_j^n$ , where the expansion coefficients whose orders are higher than  $M_j^n$  are simply cut off.

For the completeness of this paper, the detailed numerical method for the regularized method is listed in Appendix A.

## 4 Numerical Experiments

By now, we are ready to carry out our numerical tests to see the performance of the hybrid method. In order to reduce the numerical computation, the dimension reduction method in the microscopic velocity space is utilized here, which we will introduce in the next section.

## 4.1 Dimension reduction method

In some benchmark problems, for example the shock wave problem, we only focus on the spatial 1D and microscopic 3D problems. In this case, the distribution function has some symmetric properties in the direction  $v_2$  and  $v_3$ . Therefore, the dimension reduction method is always adopted to reduce the computational complexity. In this paper, the dimension reduction method in [6] is utilized for the regularized moment method, where the BGK and Shakhov collision terms are discussed. In this paper, the total freedom of the distribution function in the 3D microscopic velocity space is described by two distribution functions in 1D microscopic velocity space. The reduced distribution functions are defined

$$g(t, x, v_1) = \int_{\mathbb{R}^2} f(t, x, \mathbf{v}) dv_2 dv_3, \quad h(t, x, v_1) = \int_{\mathbb{R}^2} \frac{v_2^2 + v_3^2}{2} f(t, x, \mathbf{v}) dv_2 dv_3. \quad (4.1)$$

Assuming the expansion number of the initial distribution function  $f(t, x, \mathbf{v})$  is  $M$ , then  $g(t, x, v_1)$  and  $h(t, x, v_1)$  can be approximated as

$$g(t, x, v_1) \approx \sum_{\alpha_1 \leq M_g} g_{\alpha_1}(t, x) \mathcal{H}_{\alpha_1}^{u_1, \theta}(\xi_1), \quad h(t, x, v_1) \approx \sum_{\alpha_1 \leq M_h} h_{\alpha_1}(t, x) \mathcal{H}_{\alpha_1}^{u_1, \theta}(\xi_1), \quad \xi_1 = \frac{v_1 - u_1}{\sqrt{\theta}}, \quad (4.2)$$

where  $M_g = M$  and  $M_h = M - 2$  and  $\theta$  is the temperature of the distribution function  $f(t, x, \mathbf{v})$ . Substituting the expansion (4.2) into the Boltzmann equation, we can derive similar moment equations for  $g(t, x, v_1)$  and  $h(t, x, v_1)$ . For the reduced model, the criterion is applied to both distribution functions. Precisely, for the distribution function  $g(t, x, v_1)$ , the same criterion in the last section is adopted. For the distribution function  $h(t, x, v_1)$ , when the distribution function is Maxwellian, it equals zero. Then the criterion is changed as below: supposing the eigenvalues of the indicator matrix get by  $g(t, x, v_1)$  is  $\lambda_i, i = 1, 2, 3$ , the criterion in both regions is changed into

### From kinetic to fluid

1. the eigenvalues are all close to the eigenvalues of the Euler equations.

$$\max_{i=1,2,3} |\lambda_i - 1| \leq \epsilon_1. \quad (4.3)$$

2. the  $l_1$  norm of the expansion coefficients of the distribution function  $g_\alpha$  and  $h_\alpha$  are small.

$$\sum_{4 < |\alpha| \leq M} |g_\alpha| \leq \epsilon_2, \quad \sum_{2 < |\alpha| \leq M-2} |h_\alpha| \leq \epsilon_2. \quad (4.4)$$

### From fluid to kinetic

1. at least one of the eigenvalues is far to the eigenvalues of the Euler equations.

$$\max_{i=1,2,3} |\lambda_i - 1| > \epsilon_1. \quad (4.5)$$

Moreover, the maximum entropy method is applied on both distribution functions to complete the transition from the fluid region to the kinetic region.

## 4.2 Numerical examples

In this section, several numerical examples are tested to validate the efficiency of our hybrid algorithm. In all test cases, 1D in spatial space and 3D in microscopic velocity space problems are studied. The BKG or Shakhov collision operators are adopted with the relaxation time corresponding to the Maxwell molecules model with  $\omega$ . Thus (2.13) is reduced into

$$\tau = \frac{K_n}{\rho}. \quad (4.6)$$

The reference solution is computed by the discrete velocity method with mesh fine enough. When simulating with HME and our hybrid method, the linear reconstruction in the spatial space [8] is applied to improve the efficiency of the numerical scheme and the time step is determined by the CFL condition (A.10) for all the examples. Computations for the Euler solutions, HME and hybrid method are performed in sequential code on a computer with Intel i7-7500U CPU and 16 GB memory.

### 4.2.1 Shock tube problem

This section considers the shock tube problem for the BGK collision term. The computation domain is infinite but taken to be  $[-1.5, 1.5]$  in the simulations. As in [37], the initial condition is  $f(0, x, \mathbf{v}) = f_M(\rho, u_1, \theta)$ , with

$$\rho(0, x) = \begin{cases} 7.0, & \text{if } x < 0, \\ 1.0, & \text{if } x > 0, \end{cases} \quad p(0, x) = \rho\theta = \begin{cases} 7.0, & \text{if } x < 0, \\ 1.0, & \text{if } x > 0, \end{cases} \quad u_x(0, x) = 0. \quad (4.7)$$

We consider different Knudsen numbers ranging from the kinetic regime to the fluid limit. The numerical solutions get by the hybrid method and HME are studied, where the numerical solutions to Euler equations and that to Boltzmann equation get by DVM is also computed as reference. In all these computations, we take 1000 evenly spaced grids in spatial space for both the hybrid method and HME, while the Euler solution is computed on a sufficiently fine mesh to ensure convergence. For the full HME system and the hybrid model, the maximum expansion order is set as  $M = 40$ . The ending time is  $t = 0.3$ . In our test, the Knudsen number is set as  $Kn = 0.0001, 0.05, 0.5$  and  $5$ , where the computational region is changing from the fluid regime to the kinetic regime.

In Figure 1, 2, 3 and 4, the numerical solutions of density  $\rho$ , macroscopic velocity in the  $x$ - direction  $u_x$ , temperature  $\theta$  and heat flux in the  $x$ - direction  $q_x$  for the hybrid method and HME with different Knudsen numbers are plotted. From these figures, we can see that for all these Knudsen numbers, the numerical solutions get by the hybrid method and HME are all on top of each other. Moreover, they are all matching well with the reference solutions get by DVM. It means that the hybrid method could capture the movement of the particles for all the regimes. Especially, when  $Kn = 0.0001$  where it belongs to the fluid regime, it is expected that Euler equations could describe the movement of the particles. From Figure 1, we can see that the numerical solutions of the hybrid method and HME are all consistent with that of the Euler equation. With the increasing of the Knudsen number, the numerical solutions are moving further and further away from that of the Euler equations. When  $Kn = 5$ , the particles are in the transitional area, and can only be described by the kinetic theory. From Figure 4, we can find that numerical solutions of the hybrid method and HME are still almost the same, but all these solutions are quite different from that of Euler equations.

In order to show the efficiency of the hybrid method, the time variation of the expansion order for each grid used by the hybrid method at each time step is tested. Figure 5 shows the change of the expansion order, where the blue region is those with order 4 and the yellow region is those with order 40. From it, we can find that when  $Kn = 0.0001$ , most of the regions is blue, which means that the particles are in the fluid regime. With the increasing of  $Kn$ , the yellow region is becoming bigger and bigger. From the numerical results in Figure 1 to 4, we can find that for all the Knudsen number tested, the middle part of the spatial area belongs to the kinetic regime, which is also consistent with the expansion order showed in Figure 5, which indicates that this hybrid method could exactly detect different regimes. The computation time for the hybrid method and HME for the different Knudsen numbers is compared in Table 1. We could see that the hybrid method could save the computational time for all the Knudsen numbers, which means that the hybrid method works with a high efficiency in all the regimes. For the fluid regime, the hybrid method saves up to almost half of the computation cost. Even for  $Kn = 5$  when we are in a rarefied regime, the hybrid solver reduces the computation cost by around 30 percent.

$Kn$	Full HME	Hybrid
0.0001	223s	112s
0.05	220s	143s
0.5	221s	152s
5	222s	153

Table 1: Comparison of computational time of the hybrid method and HME with different Knudsen numbers in Sec 4.2.1.

### 4.2.2 Shock tube problem with two rarefaction waves

The shock tube problem with two rarefaction waves is tested in this section, a similar set-up could be found in [2]. The computation domain is infinite but taken to be  $[-1.5, 1.5]$  in the simulation. The initial

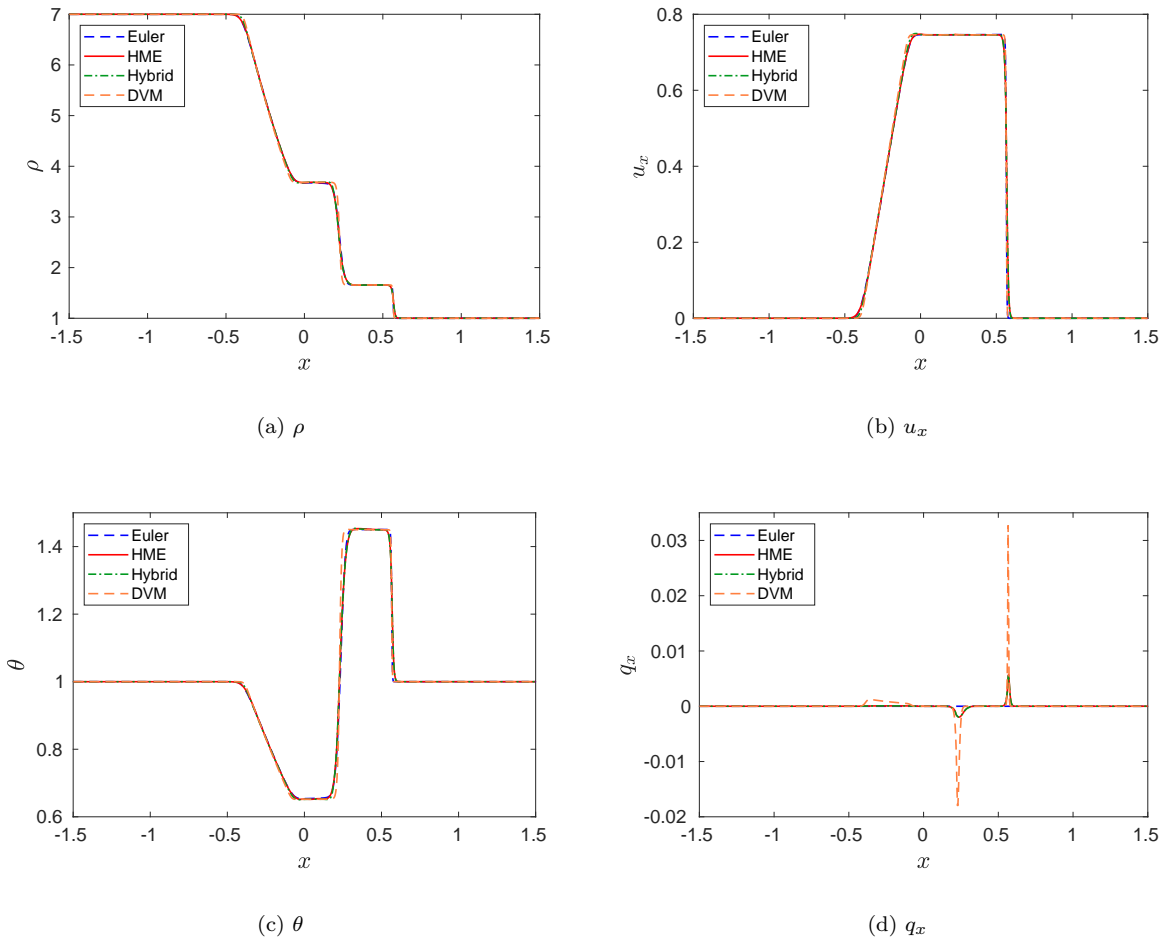
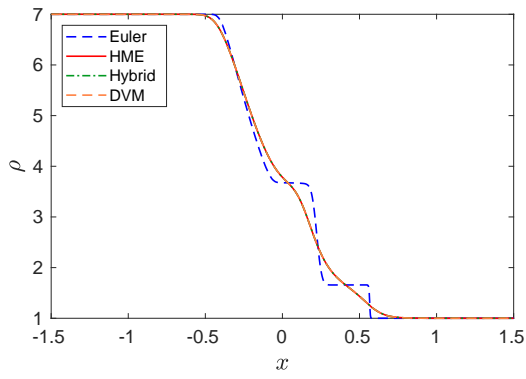
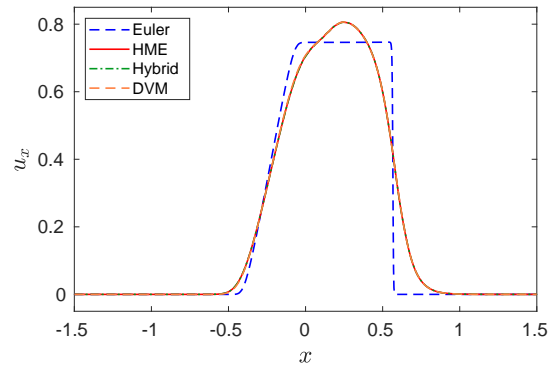


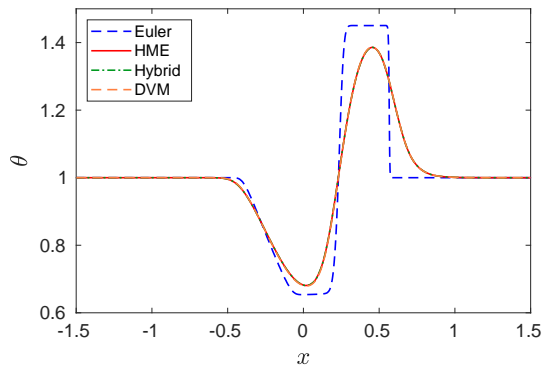
Figure 1: Comparisons of solutions in Sec 4.2.1 for  $\rho$ ,  $u_x$ ,  $\theta$  and  $q_x$  as functions of  $x$  for  $Kn = 10^{-4}$ .



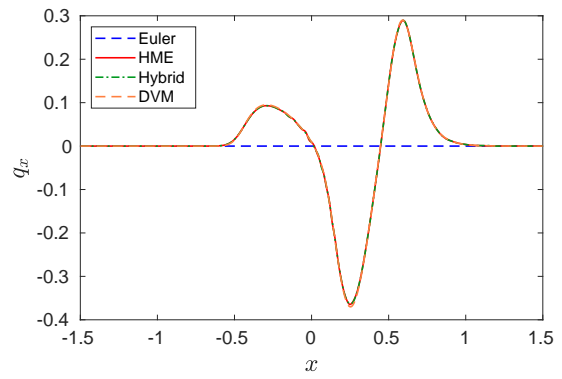
(a)  $\rho$



(b)  $u_x$



(c)  $\theta$



(d)  $q_x$

Figure 2: Comparisons of solutions in Sec 4.2.1 for  $\rho$ ,  $u_x$ ,  $\theta$  and  $q_x$  as functions of  $x$  for  $Kn = 0.05$ .

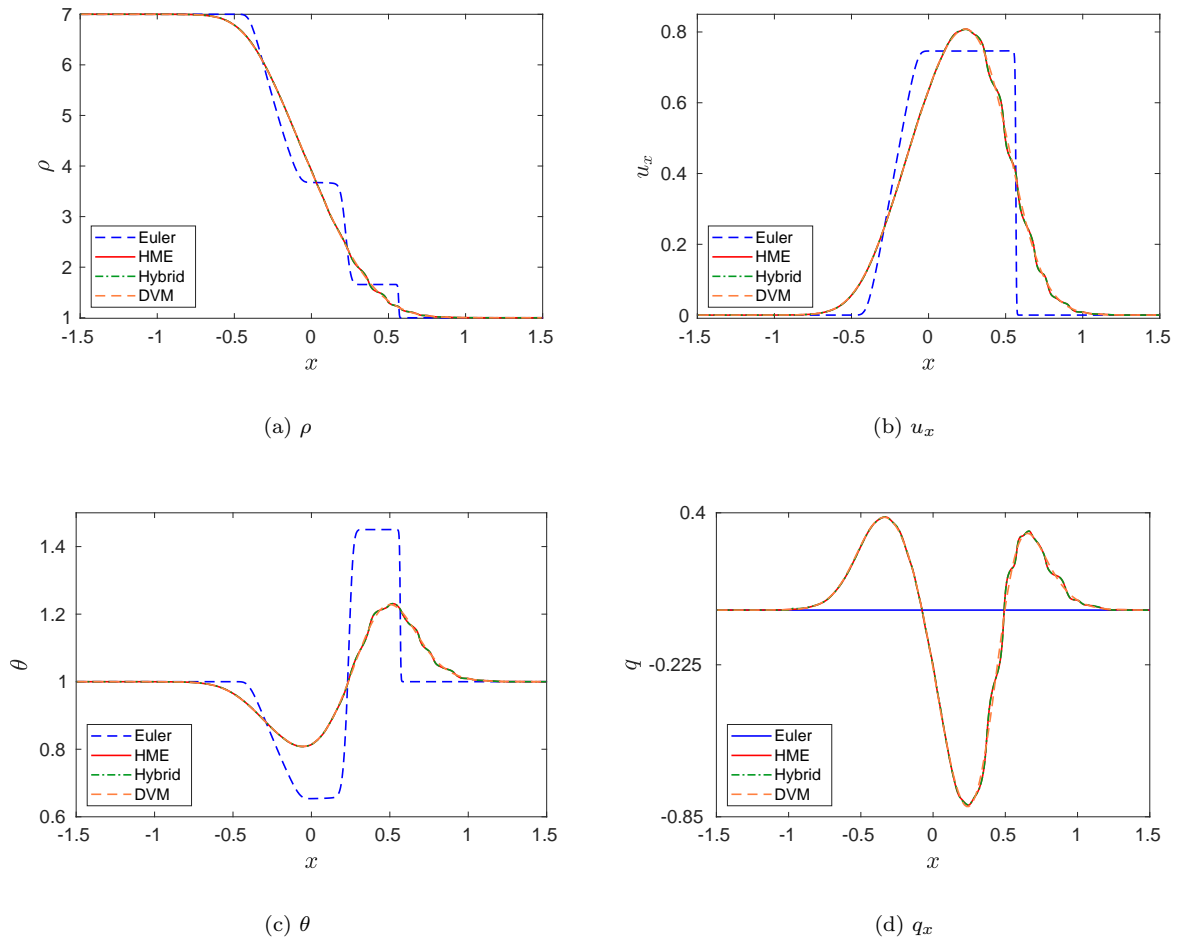


Figure 3: Comparisons of solutions in Sec 4.2.1 for  $\rho$ ,  $u_x$ ,  $\theta$  and  $q_x$  as functions of  $x$  for  $Kn = 0.5$ .

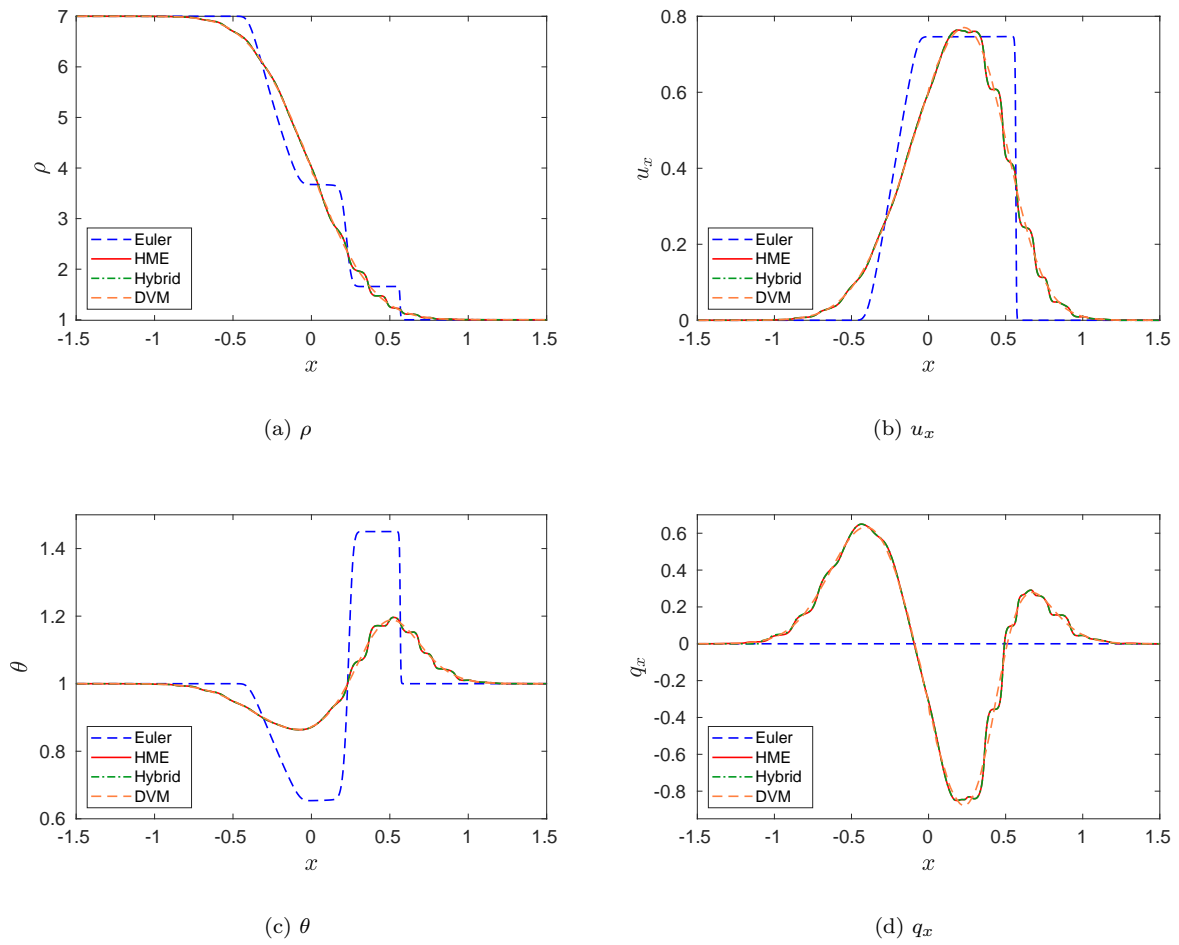
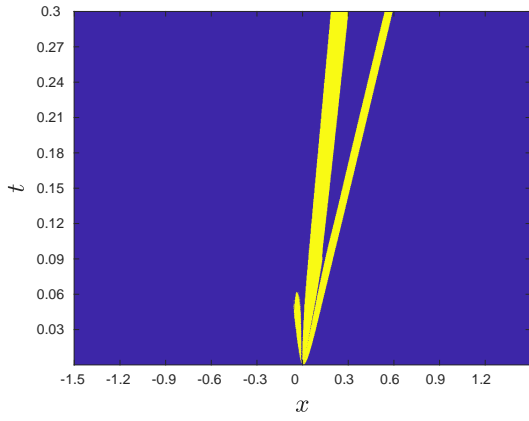
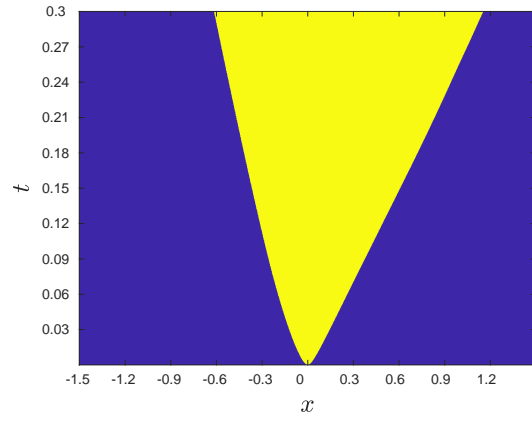


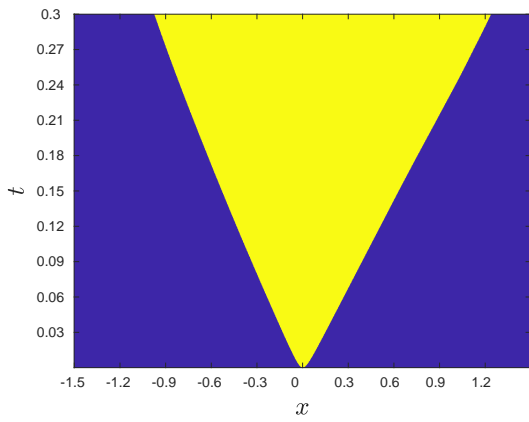
Figure 4: Comparisons of solutions in Sec 4.2.1 for  $\rho$ ,  $u_x$ ,  $\theta$  and  $q_x$  as functions of  $x$  for  $Kn = 5$ .



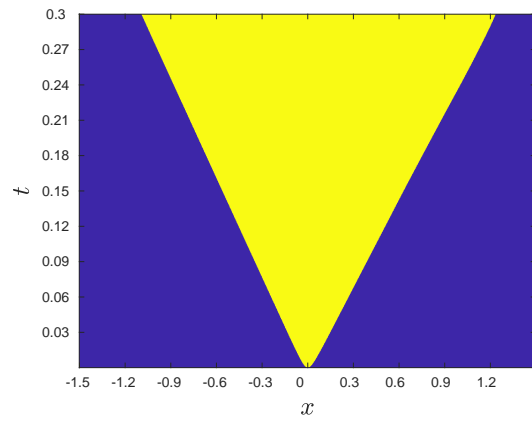
(a)  $Kn = 0.0001$



(b)  $Kn = 0.05$



(c)  $Kn = 0.5$



(d)  $Kn = 5$

Figure 5: The maximum order used in each region at each time step for different Knudsen numbers in Sec 4.2.1.

condition is  $f(0, x, \mathbf{v}) = f_M(\rho, u_x, \theta)$ , with

$$\rho(0, x) = 1.0, \quad u_x(0, x) = \begin{cases} -1.0, & \text{if } x < 0, \\ 1.0, & \text{if } x > 0, \end{cases} \quad \theta = 1.0. \quad (4.8)$$

We take  $Kn = 0.01$  and  $Kn = 1$  respectively and compare the different solutions for the Shakhov collision operator. In the test, the grid size is set as  $N = 1000$  and the maximum expansion order is  $M = 40$ .

Figure 6 and 7 show the macroscopic variables  $\rho$ ,  $u_x$ ,  $\theta$  and  $q_x$  at  $t = 0.12$  with different Knudsen numbers. For both Knudsen number, we can find that the numerical solutions get by the hybrid method are almost the same as HME, which all agree with the reference get by DVM. This means that for problems with two rarefaction waves, the hybrid method can capture the movement of the particles for all the regimes.

The efficiency of the hybrid method is also tested. Figure 8 shows the time evolution of the maximum order actually used by the hybrid method at each time step for each grid in this example. As in the previous example, the blue region indicates a maximum expansion order of 4, while the yellow region means a maximum expansion order of 40. From it, we can find that in the middle of the spatial area, where it is the kinetic regime, the expansion order is 40, while in the left and right sides of the spatial area, the expansion order four is kept. All this means that the hybrid scheme could detect the rarefied zones correctly for the rarefaction wave problems. In Subsection 4.2.2 we compare the computation time for the hybrid method and HME for the two Knudsen numbers we tested. For both cases, we see that almost 50 percent of reduction in computation cost, which shows the high efficiency of the hybrid method.

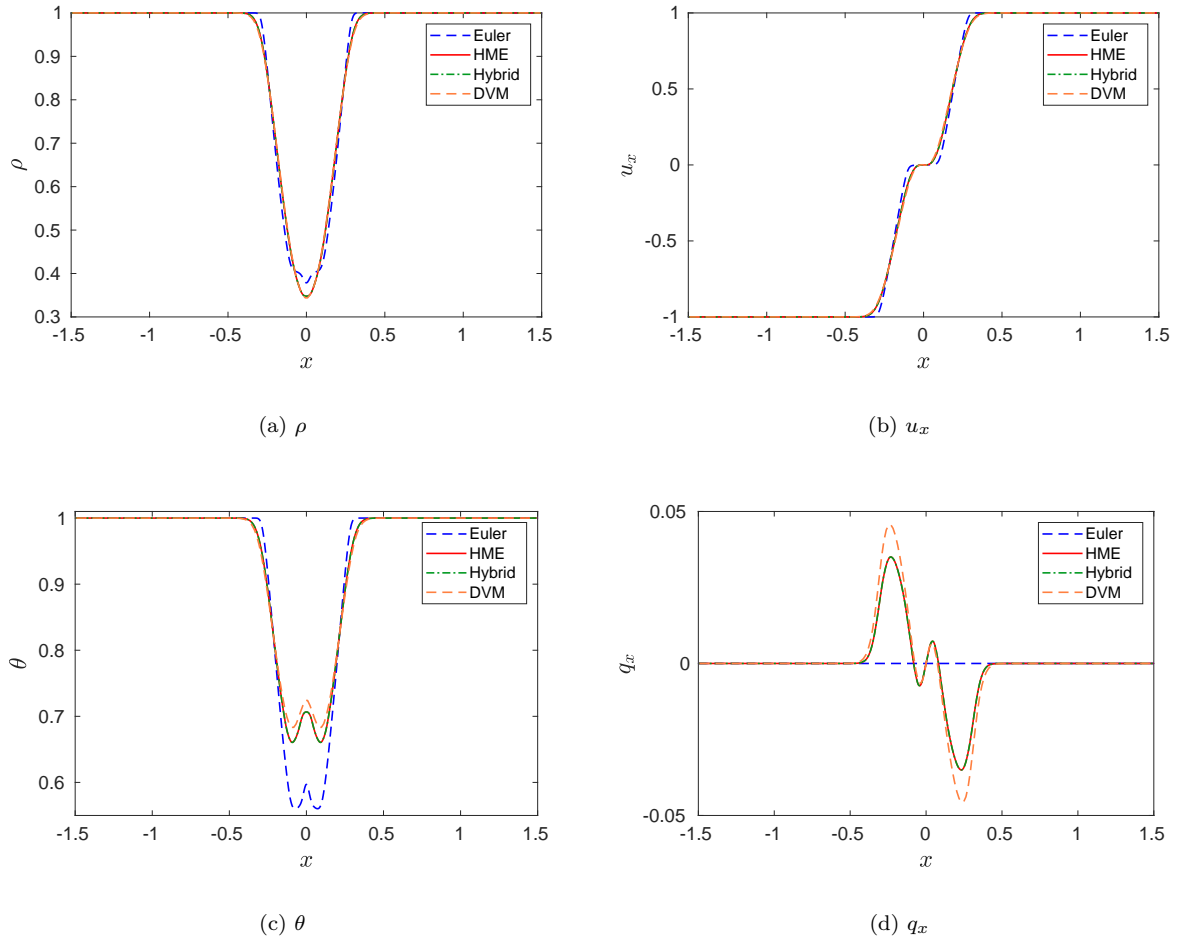


Figure 6: Comparisons of solutions for  $\rho$ ,  $u_x$ ,  $\theta$  and  $q_x$  as functions of  $x$  for  $Kn = 0.01$  in Sec 4.2.2.

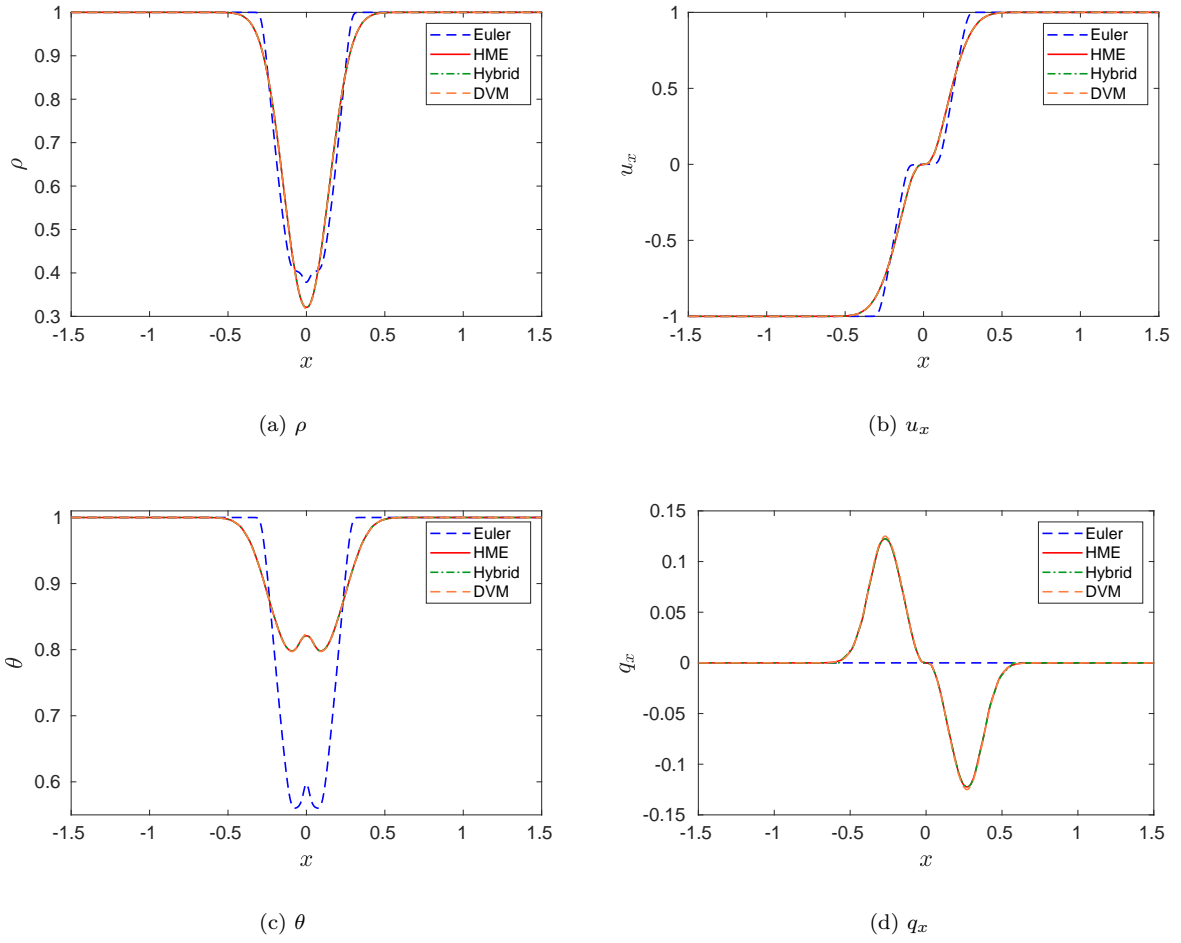


Figure 7: Comparisons of solutions for  $\rho$ ,  $u_x$ ,  $\theta$  and  $q_x$  as functions of  $x$  for  $Kn = 1$  in Sec 4.2.2.

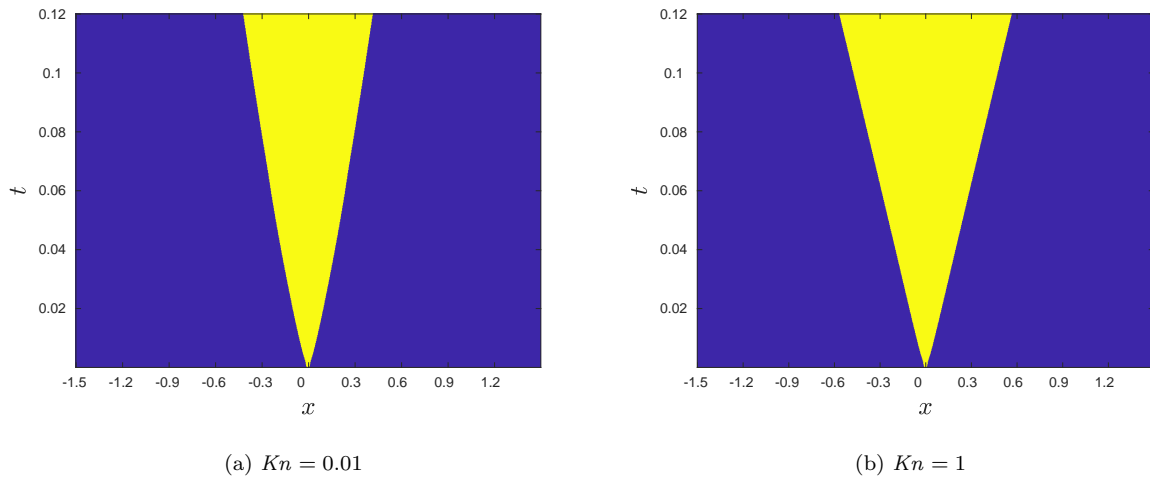


Figure 8: The maximum order used in each spatial grid at each time step for different Knudsen numbers in Sec 4.2.2.

$Kn$	Full HME	Hybrid
0.01	74s	43s
1	75s	44s

Table 2: Comparison of computational time of the hybrid method and HME with different Knudsen numbers in Sec 4.2.2.

### 4.2.3 Blast wave

In this section, a similar blast wave problem as in [14] is tested. The computation domain is taken to be  $[-1, 1]$  in the simulations. The initial condition is  $f(0, x, \mathbf{v}) = f_M(\rho, u_x, \theta)$ , with

$$\rho(0, x) = 1.0, \quad u_x(0, x) = \begin{cases} 1.0, & \text{if } x \leq -0.3, \\ 0, & \text{if } -0.3 < x < 0.3, \\ -1.0, & \text{if } x \geq 0.3, \end{cases} \quad \theta = \begin{cases} 1.5, & \text{if } x \leq -0.3, \\ 1.0, & \text{if } -0.3 < x < 0.3, \\ 1.5, & \text{if } x \geq 0.3. \end{cases} \quad (4.9)$$

We take  $Kn = 0.001$  and  $Kn = 0.01$ . In the test, the grid size is set as  $N = 1000$  and the maximum expansion order is  $M = 40$ .

Figure 9 and 10 show the behavior of  $\rho$ ,  $u_x$ ,  $\theta$  and  $q_x$  at time  $t = 0.05, 0.15$  and  $0.35$  for the Knudsen number  $Kn = 0.001$  and  $0.01$ . For all these cases, we see good agreement between the hybrid solver and HME, as well as the reference solution. When  $Kn$  is small, we can find that the numerical solutions of HME and hybrid agree well with that of Euler equations. In Figure 11, the time evolution of the maximum order actually used by the hybrid method is again plotted. We can find that for the kinetic region in the middle of the spatial space, the expansion order is 40, which is the yellow region. For the fluid regime, the expansion order is 4, which is the blue region. Note that when  $Kn = 0.001$ , the spatial position of the yellow region changes as time evolves. This is probably because the relaxation time depends on  $Kn/\rho$ , and as shown in Figure 9, the position of the peak values of  $\rho$  changes in space with time evolution. This shows our hybrid method could detect the fluid and kinetic regimes nicely. Moreover, when  $Kn = 0.001$ , the blue region with expansion order 4 is much larger than that of  $Kn = 0.01$ , which means that more area belongs to the fluid regime when Knudsen number is smaller. Subsection 4.2.3 compares the computation cost of the hybrid method and HME, where we could see a significant reduction in computation cost. Moreover, when  $Kn = 0.001$ , the hybrid method is more efficient than the case  $Kn = 0.01$ , which is also consistent with the knowledge perception and the variation of the expansion order as time going.

$Kn$	0.001			0.01		
	$t_{end}$	HME (s)	Hybrid (s)	$t_{end}$	HME	Hybrid (s)
	0.05	61	35	0.05	59	35
	0.05	175	108	0.15	181	125
	0.35	403	264	0.35	422	336

Table 3: Comparison of computational time of the hybrid method and HME at different time for different  $Kn$  in Sec 4.2.3.

## 5 Conclusion

This work aims at a uniform hybrid moment method for the multi-scale kinetic problems. The method is proposed in the framework of the regularized moment method. Instead of Euler or Navier-Stokes equations, the fourth order moment system is utilized as the governing equations in the fluid region, in which case only one set of the numerical scheme is needed for both fluid and kinetic regions. Moreover, with the fourth order moment systems, the maximum entropy method is applied here to derive the high order expansion coefficients of the distribution function in the interface area from the fluid regime to the kinetic regime. Several numerical experiments show that this hybrid numerical algorithm can capture the movement of the particles in different regions accurately and efficiently.

The method will be further validated in the numerical tests for more complex kinetic models, which is one of the ongoing work. The extension of the method for transferring information from kinetic to fluid regime to higher dimensional problems will also be studied in future work.

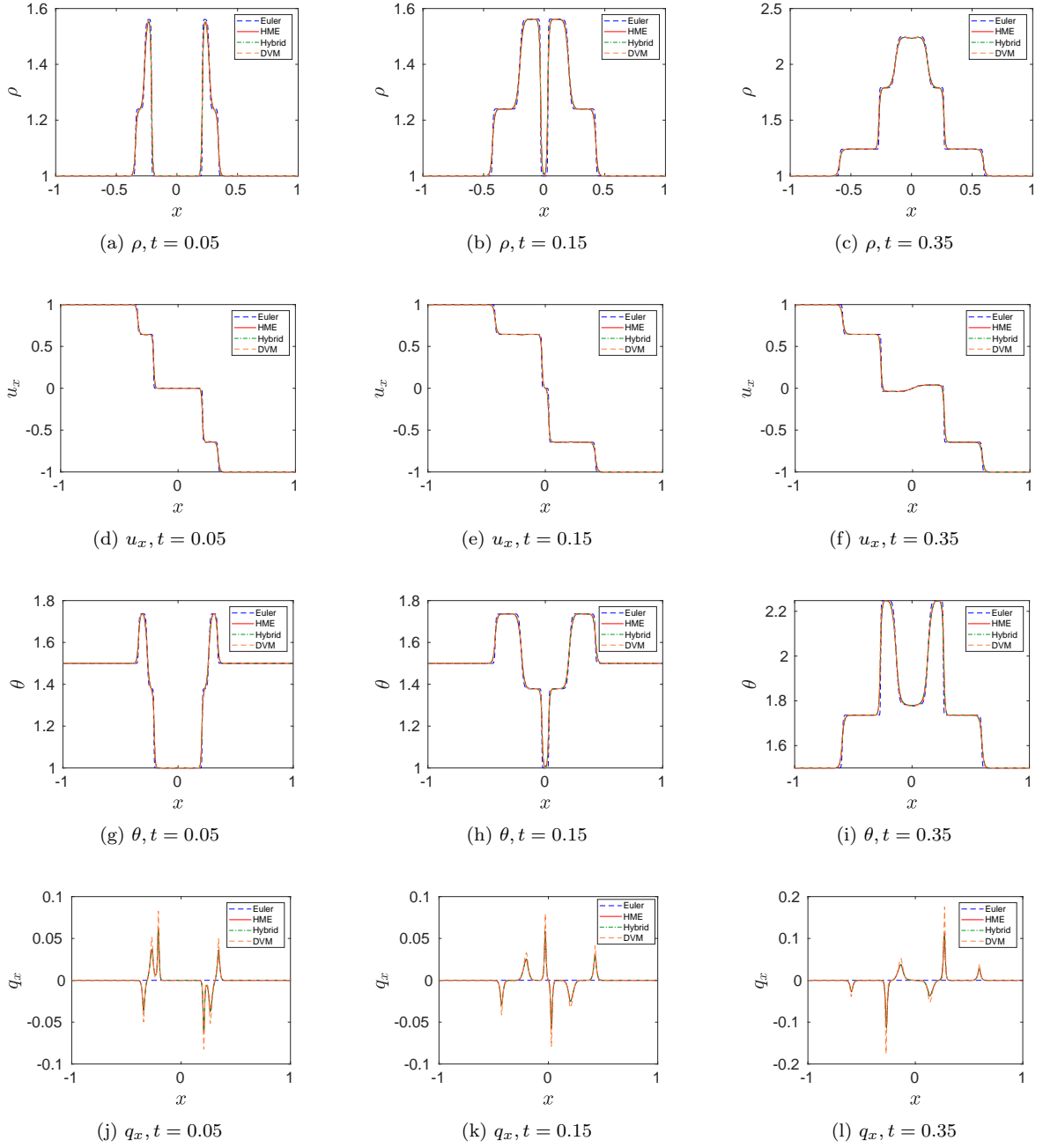


Figure 9: Comparisons of solutions for  $\rho$ ,  $u_x$ ,  $\theta$  and  $q_x$  as functions of  $x$  for  $Kn = 0.001$  at time  $t = 0.05, 0.15$  and  $0.35$  in Sec 4.2.3.

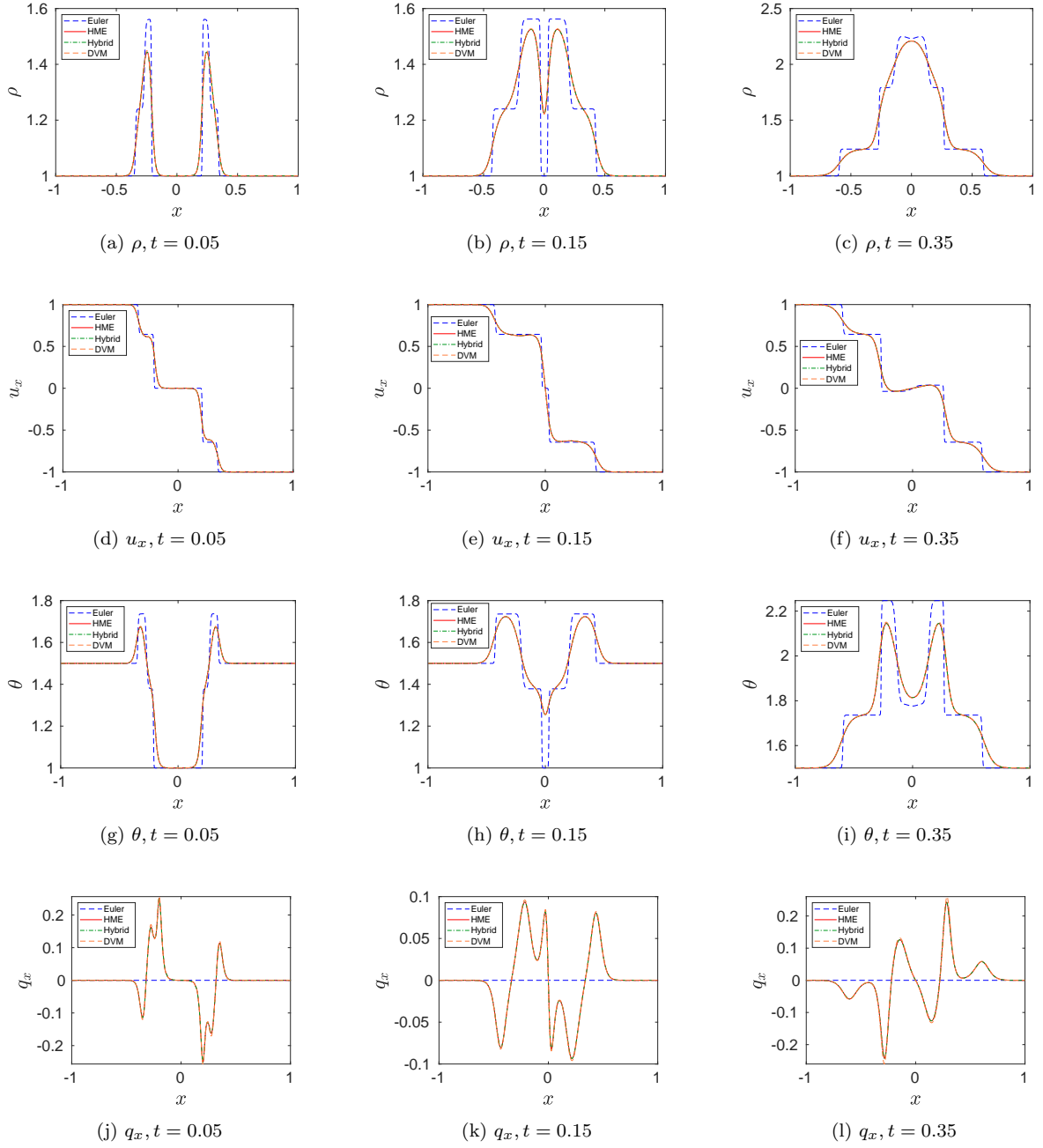


Figure 10: Comparisons of solutions for  $\rho$ ,  $u_x$ ,  $\theta$  and  $q_x$  as functions of  $x$  for  $Kn = 0.01$  at time  $t = 0.05, 0.15$  and  $0.35$  in Sec 4.2.3.

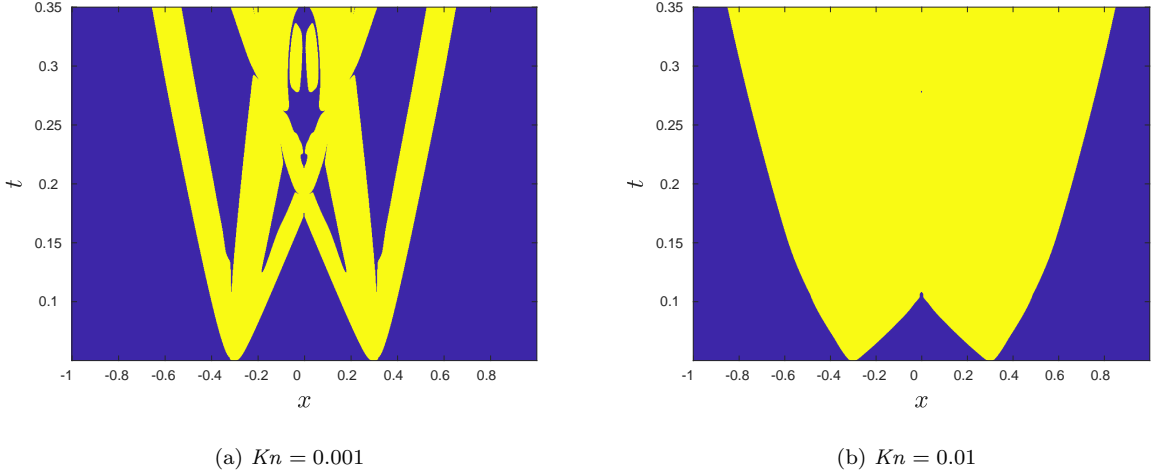


Figure 11: The maximum order used in all spatial grids at each time step for different Knudsen numbers in Sec 4.2.3.

## Acknowledgements

We thank Prof. Ruo Li from Peking University for his valuable suggestions to this research project. This research of Weiming Li is supported in part by Science Challenge Project (NO. TZ2016002). The research of Peng Song is supported in part by the Natural Science Foundation of China (91630310) and the CAEP foundation (No.CX20200026). And that of Y. Wang is supported in part by Science Challenge Project (NO. TZ2016002) and the Natural Science Foundation of China (U1930402).

## A Numerical scheme for the regularized moment method

In this section, we will introduce the numerical scheme of the dimensional reduced regularized moment method. We refer readers [6] for more details. Let  $\omega = (\omega^{(g)}, \omega^{(h)})$  be the variables of the reduced system, where  $\omega^{(f)}$ ,  $f = g, h$  is the corresponding variable  $\omega$  of the distribution function  $f$  in (2.28). The reduced moment system is written as

$$\frac{\partial \omega}{\partial t} + \sum_{j=1}^2 \mathbf{B}_j \frac{\partial \omega}{\partial x} = \mathbf{Q}\omega. \quad (\text{A.1})$$

Splitting method is adopted to solve (A.1), which is split into the convection part and the collision part

- convection part:

$$\frac{\partial \omega}{\partial t} + \sum_{j=1}^2 \mathbf{B}_j \frac{\partial \omega}{\partial x} = 0. \quad (\text{A.2})$$

- collision part:

$$\frac{\partial \omega}{\partial t} = \mathbf{Q}\omega. \quad (\text{A.3})$$

The detailed algorithm is as below,

1. Let  $n = 0$ , and give the initial value of  $\omega_i^n$ .
2. Calculate the time step length  $\Delta t_n$  by CFL condition.
3. Solve the convection part using the finite volume method with the HLL flux, and denote the result by  $\omega_i^{n,*}$ . The detailed distribution function in the hybrid method is given in algorithm 3.2.
4. Update the collision step using  $\omega_i^{n,*}$  as the initial condition.
5. Let  $t \leftarrow t + \Delta t_n$  and  $n \leftarrow n + 1$ ; then go to Step 2.

The numerical scheme for the convection step and the collision is listed below in detail.

**Convection step** For the convection part, the moment equation (A.2) is reformulated as

$$\frac{\partial \boldsymbol{\omega}}{\partial t} + \frac{\partial \mathbf{F}(\boldsymbol{\omega})}{\partial x} + \mathbf{R}(\boldsymbol{\omega}) \frac{\partial \boldsymbol{\omega}}{\partial x} = 0. \quad (\text{A.4})$$

The finite volume method is utilized here. Precisely

$$\boldsymbol{\omega}_i^{n,*} = \boldsymbol{\omega}_i^n - \frac{\Delta t_n}{\Delta x} \left( \hat{\mathbf{F}}_{i+1/2}^n - \hat{\mathbf{F}}_{i-1/2}^n \right) - \frac{\Delta t_n}{\Delta x} \left( \hat{\mathbf{R}}_{i+1/2}^{n-} - \hat{\mathbf{R}}_{i-1/2}^{n+} \right), \quad (\text{A.5})$$

where  $\hat{\mathbf{F}}_{i+1/2}^n$  is the HLL numerical flux defined by

$$\hat{\mathbf{F}}_{i+1/2}^n = \begin{cases} \mathbf{F}(\boldsymbol{\omega}_i^n), & \lambda_{i+1/2}^{L,n} \geq 0, \\ \frac{\lambda_{i+1/2}^{R,n} \mathbf{F}(\boldsymbol{\omega}_i^n) - \lambda_{i+1/2}^{L,n} \mathbf{F}(\boldsymbol{\omega}_{i+1}^n)}{\lambda_{i+1/2}^{R,n} - \lambda_{i+1/2}^{L,n}} + \frac{\lambda_{i+1/2}^{L,n} \lambda_{i+1/2}^{R,n} (\boldsymbol{\omega}_{i+1}^n - \boldsymbol{\omega}_i^n)}{\lambda_{i+1/2}^{R,n} - \lambda_{i+1/2}^{L,n}}, & \lambda_{i+1/2}^{L,n} < 0 < \lambda_{i+1/2}^{R,n}, \\ \mathbf{F}(\boldsymbol{\omega}_{i+1}^n), & \lambda_{i+1/2}^{R,n} \leq 0. \end{cases} \quad (\text{A.6})$$

The numerical flux for the nonconservation part  $\hat{\mathbf{R}}_{i+1/2}^{n\pm}$  is defined by

$$\hat{\mathbf{R}}_{i+1/2}^{n-} = \begin{cases} 0, & \lambda_{i+1/2}^{L,n} \geq 0, \\ -\frac{\lambda_{i+1/2}^{L,n}}{\lambda_{i+1/2}^{R,n} - \lambda_{i+1/2}^{L,n}} \mathbf{g}_{i+1/2}^n, & \lambda_{i+1/2}^{L,n} < 0 < \lambda_{i+1/2}^{R,n}, \\ \mathbf{g}_{i+1/2}^n, & \lambda_{i+1/2}^{R,n} \leq 0, \end{cases} \quad (\text{A.7})$$

$$\hat{\mathbf{R}}_{i+1/2}^{n+} = \begin{cases} -\mathbf{g}_{i+1/2}^n, & \lambda_{i+1/2}^{L,n} \geq 0, \\ -\frac{\lambda_{i+1/2}^{R,n}}{\lambda_{i+1/2}^{R,n} - \lambda_{i+1/2}^{L,n}} \mathbf{g}_{i+1/2}^n, & \lambda_{i+1/2}^{L,n} < 0 < \lambda_{i+1/2}^{R,n}, \\ 0, & \lambda_{i+1/2}^{R,n} \leq 0, \end{cases}$$

with

$$\mathbf{g}_{i+1/2}^n = \int_0^1 \mathbf{R}(\Phi(s; \mathbf{q}_i^n; \mathbf{q}_{i+1}^n)) \frac{\partial \Phi}{\partial s}(s; \mathbf{q}_i^n; \mathbf{q}_{i+1}^n) ds, \quad (\text{A.8})$$

where  $\Phi(s; \cdot, \cdot)$  is a path to connect the two states. We refer [9] for more details. The characteristic speeds  $\lambda_{i+1/2}^R$  and  $\lambda_{i+1/2}^L$  are

$$\begin{aligned} \lambda_{i+1/2}^{R,n} &= \max \left( u_{1,i}^n + C_{M+1} \sqrt{\theta_i^n}, u_{1,j}^n + C_{M+1} \sqrt{\theta_{i+1}^n} \right), \\ \lambda_{i+1/2}^{L,n} &= \max \left( u_{1,i}^n - C_{M+1} \sqrt{\theta_i^n}, u_{1,j}^n - C_{M+1} \sqrt{\theta_{i+1}^n} \right), \end{aligned} \quad (\text{A.9})$$

where  $C_{M+1}$  is the maximal roots of the  $M+1$  degree Hermite polynomial. The time step length is also decided by the characteristic velocity as

$$\frac{\Delta t^n \max_i \left\{ \left| \lambda_{i+1/2}^{R,n} \right|, \left| \lambda_{i+1/2}^{L,n} \right| \right\}}{\Delta x} \leq \text{CFL}. \quad (\text{A.10})$$

**Collision step** For the BGK and Shakhov model, the collision part can be solved exactly in the reduced regularized moment method. For neatness, the superscript  $n$ ,  $n+1$  and the subscripts  $i$  are omitted. The solutions are as below:

- For the BGK model:

$$\begin{aligned} g_\alpha &= g_\alpha^* \exp \left( -\frac{\Delta t}{\tau} \right), \quad 2 \leq |\alpha| \leq M, \\ h_0 &= g_0^* \theta^* \left( 1 - \exp \left( \frac{\Delta t}{\tau} \right) \right) + h_0^* \exp \left( -\frac{\Delta t}{\tau} \right), \\ h_\alpha &= h_\alpha^* \exp \left( -\frac{\Delta t}{\tau} \right), \quad 1 \leq |\alpha| \leq M-2. \end{aligned} \quad (\text{A.11})$$

- For the Shakhov model:

$$\begin{aligned}
g_{3e_1} &= g_{3e_1}^* \exp\left(-\frac{\Delta t}{\tau}\right) + \frac{1}{5} q_i^* \left( \exp\left(-\frac{\text{Pr} \Delta t}{\tau}\right) - \exp\left(-\frac{\Delta t}{\tau}\right) \right), \\
g_\alpha &= g_\alpha^* \exp\left(-\frac{\Delta t}{\tau}\right), \quad |\alpha| = 2 \text{ or } 4 \leq |\alpha| \leq M, \\
h_0 &= g_0^* \theta^* \left( 1 - \exp\left(\frac{\Delta t}{\tau}\right) \right) + h_0^* \exp\left(-\frac{\Delta t}{\tau}\right), \\
h_{e_1} &= h_{e_1}^* \exp\left(-\frac{\Delta t}{\tau}\right) + \frac{1}{5} q_i^* \left( \exp\left(-\frac{\text{Pr} \Delta t}{\tau}\right) - \exp\left(-\frac{\Delta t}{\tau}\right) \right), \\
h_{3e_1} &= h_{3e_1}^* \exp\left(-\frac{\Delta t}{\tau}\right) + \frac{\theta^*}{5} q_i^* \left( \exp\left(-\frac{\text{Pr} \Delta t}{\tau}\right) - \exp\left(-\frac{\Delta t}{\tau}\right) \right), \\
h_\alpha &= h_\alpha^* \exp\left(-\frac{\Delta t}{\tau}\right), \quad |\alpha| = 2 \text{ or } 4 \leq |\alpha| \leq M - 2.
\end{aligned} \tag{A.12}$$

## B Algorithm for the maximum entropy closure

This section introduces the numerical scheme for solving the specific maximum entropy distribution function needed in our hybrid moment method. More details of this algorithm are the subject of a subsequent article.

With the dimension reduction method in the microscopic velocity space, the fourth order moment in 1D microscopic velocity space is utilized in the fluid regime. Consider the maximum entropy moment problem

$$\hat{f} = \operatorname{argmin} \int_{\mathbb{R}} f \log f - f \, dv, \quad \text{s.t.} \langle \hat{f}(v) \rangle_k = \mu_k, \quad k = 0, \dots, 4. \tag{B.1}$$

We follow the same approach as [1] to reformulate Equation (B.1) into the unconstrained form

$$\mathcal{L}(\boldsymbol{\lambda}) = \int_{\mathbb{R}} \exp\left(\sum_{i=0}^4 \lambda_i v^i\right) - \sum_{i=0}^4 \lambda_i \mu_i, \tag{B.2}$$

which we solve using the Newton algorithm. The structure of the Newton algorithm we employ is as follows:

1. Provide the starting point  $\boldsymbol{\lambda}_0$  by a combination of analysis and interpolation from pre-computed data. Compute the corresponding gradient  $(\nabla \mathcal{L})_0$  and Hessian matrix  $H_0$ .
2. At iteration  $m$ , perform the following steps:

- (a) Solve for the direction of descent by

$$H_m \mathbf{d}_m = -(\nabla \mathcal{L})_m;$$

- (b) Find the next iteration point  $\boldsymbol{\lambda}_{m+1}$  as

$$\boldsymbol{\lambda}_{m+1} = \boldsymbol{\lambda}_m + \mathbf{d}_m;$$

- (c) At the new iteration point  $\boldsymbol{\lambda}_{m+1}$ , compute the gradient  $(\nabla \mathcal{L})_{m+1}$  and the Hessian  $H_{m+1}$ .

Direct computation shows that

$$(\nabla \mathcal{L})_{m,j} = \int_{\mathbb{R}} v^j \exp\left(\sum_{i=0}^4 \lambda_i v^i\right) - \mu_j, \quad H_{m,jk} = \int_{\mathbb{R}} v^{i+j} \exp\left(\sum_{i=0}^4 \lambda_i v^i\right) \, dv. \tag{B.3}$$

Therefore most of the computation effort in solving the optimization problem lies in computing the moments from the current iteration of the Lagrange multipliers. In our computation, we utilize the fact that the maximum entropy distribution function for fourth order system either contains one peak or two peaks, therefore we employ a cutoff function to approximate sufficiently accurately the integration on  $\mathbb{R}$  by integration on one or two finite domains. A standard Gauss-Chebyshev quadrature is then employed for computation of the integration on the finite domains.

## References

- [1] R. Abramov et al. The multidimensional maximum entropy moment problem: A review of numerical methods. *Commun. Math. Sci.*, 8(2):377–392, 2010.
- [2] A. Alessandro and P. Gabriella. A hybrid method for hydrodynamic-kinetic flow-Part II-Coupling of hydrodynamic and kinetic models. *J. Comput. Phys.*, 231(16):5217 – 5242, 2012.
- [3] G. Bird. *Molecular Gas Dynamics and the Direct Simulation of Gas Flows*. Oxford: Clarendon Press, 1994.
- [4] E. Caffisch, G. Dimarco, and L. Pareschi. An hybrid method for the Boltzmann equation. *AIP Conference Proceedings*, 1786(1):180001, 2016.
- [5] Z. Cai, Y. Fan, and R. Li. Globally hyperbolic regularization of Grad’s moment system. *Comm. Pure Appl. Math.*, 67(3):464–518, 2014.
- [6] Z. Cai, Y. Fan, R. Li, and Z. Qiao. Dimension-reduced hyperbolic moment method for the Boltzmann equation with BGK-type collision. *Commun. Comput. Phys.*, 15(5):1368–1406, 2014.
- [7] Z. Cai and R. Li. Numerical regularized moment method of arbitrary order for Boltzmann-BGK equation. *SIAM J. Sci. Comput.*, 32(5):2875–2907, 2010.
- [8] Z. Cai and M. Torrilhon. Numerical simulation of microflows using moment methods with linearized collision operator. *J. Sci. Comput.*, 74(1):336–374, 2018.
- [9] G. Dal Maso, P. Lefloch, and F. Murat. Definition and weak stability of nonconservative products. *J. Math. Pure. Appl.*, 74(6):483–548, 1995.
- [10] P. Degond, G. Dimarco, and L. Pareschi. The moment-guided Monte Carlo method. *Int. J. Numer. Meth. Fl.*, 67(2):189–213, 2011.
- [11] G. Dimarco and L. Pareschi. Hybrid multiscale methods ii. kinetic equations. *SIAM Multiscale Model Sim.*, 6(4):1169–1197, 2008.
- [12] W. Dreyer. Maximisation of the entropy in non-equilibrium. *J. Phys. A: Math. Gen.*, 20(18):6505–6517, 1987.
- [13] F. Filbet and S. Jin. A class of asymptotic preserving schemes for kinetic equations and related problems with stiff sources. *J. Comput. Phys.*, 229:7625–7648, 2010.
- [14] F. Filbet and T. Rey. A hierarchy of hybrid numerical methods for multiscale kinetic equations. *SIAM J. Sci. Comput.*, 37(3):A1218–A1247, 2015.
- [15] F. Filbet and T. Xiong. A hybrid discontinuous Galerkin scheme for multi-scale kinetic equations. *J. Comput. Phys.*, 372:841 – 863, 2018.
- [16] I. Gamba, J. Haack, C. Hauck, and J. Hu. A fast spectral method for the Boltzmann collision operator with general collision kernels. *SIAM J. Sci. Comput.*, 39(14):B658–B674, 2017.
- [17] I. Gamba, J. Haack, and J. Hu. A fast conservative spectral solver for the nonlinear Boltzmann collision operator. In J. Fan, editor, *Proceedings of the 29th International Symposium on Rarefied Gas Dynamics*, volume 1628, pages 1003–1008, 2014.
- [18] I. Gamba and S. Rjasanow. Galerkin-Petrov approach for the Boltzmann equation. *J. Comput. Phys.*, 366:341–365, 2018.
- [19] D. Goldstein, B. Sturtevant, and J. E. Broadwell. Investigations of the motion of discrete-velocity gases. *Progress in Astronautics and Aeronautics*, 117:100–117, 1989.
- [20] H. Grad. On the kinetic theory of rarefied gases. *Comm. Pure Appl. Math.*, 2(4):331–407, 1949.
- [21] C. Hauck. High-order entropy-based closures for linear transport in slab geometry. *Commun. Math. Sci.*, 9(1):187–205, 2011.

- [22] Z. Hu, R. Li, T. Lu, Y. Wang, and W. Yao. Simulation of an  $n^+ - n - n^+$  diode by using globally-hyperbolically-closed high-order moment models. *J. Sci. Comput.*, 59(3):761–774, 2014.
- [23] E. Jaynes. Information theory and statistical mechanics. *Phys. Rev.*, 106(4):620, 1957.
- [24] V. Kolobov, R. Arslanbekov, V. Aristov, A. Frolova, and S. Zabelok. Unified solver for rarefied and continuum flows with adaptive mesh and algorithm refinement. *J. Comput. Phys.*, 223(2):589 – 608, 2007.
- [25] C. Levermore. Moment closure hierarchies for kinetic theories. *J. Stat. Phys.*, 83(5–6):1021–1065, 1996.
- [26] C. Levermore, J. Morokoff, and B. Nadiga. Moment realizability and the validity of the NavierStokes equations for rarefied gas dynamics. *Phys. Fluids*, 10(12):3214–3226, 1998.
- [27] J. McDonald and C. Groth. Towards realizable hyperbolic moment closures for viscous heat-conducting gas flows based on a maximum-entropy distribution. *Continuum Mech. Thermodyn.*, 25(5):573–603, 2013.
- [28] J. McDonald and C. Groth. Towards realizable hyperbolic moment closures for viscous heat-conducting gas flows based on a maximum-entropy distribution. *Continuum Mech. Therm.*, 25(5):573–603, 2013.
- [29] C. Mouhot and L. Pareschi. Fast algorithms for computing the Boltzmann collision operator. *Math. Comp.*, 75(256):1833–1852, 2006.
- [30] I. Müller and T. Ruggeri. *Extended Thermodynamics*, volume 37 of *Springer tracts in natural philosophy*. Springer-Verlag, New York, 1993.
- [31] A. Panferov and A. Heintz. A new consistent discrete-velocity model for the Boltzmann equation. *Math. Method Appl. Sci.*, 25(7):571–593, 2002.
- [32] L. Pareschi and B. Perthame. A fourier spectral method for homogeneous Boltzmann equations. *Transport Theor. Stat.*, 25(3-5):369–382, 1996.
- [33] R. Schaerer, P. Bansal, and M. Torrilhon. Efficient algorithms and implementations of entropy-based moment closures for rarefied gases. *J. Comput. Phys.*, 340:138–159, 2017.
- [34] H. Struchtrup. Derivation of 13 moment equations for rarefied gas flow to second order accuracy for arbitrary interaction potentials. *SIAM Multiscale Model. Simul.*, 3(1):221–243, 2005.
- [35] H. Struchtrup and M. Torrilhon. Higher-order effects in rarefied channel flows. *Phys. Rev. E*, 78:046301, Oct 2008.
- [36] S. Tiwari. Coupling of the Boltzmann and Euler equations with automatic domain decomposition. *J. Comput. Phys.*, 144(2):710 – 726, 1998.
- [37] M. Torrilhon. Two dimensional bulk microflow simulations based on regularized Grad’s 13-moment equations. *SIAM Multiscale. Model. Simul.*, 5(3):695–728, 2006.
- [38] Y. Wang and Z. Cai. Approximation of the Boltzmann collision operator based on Hermite spectral method. *J. Comput. Phys.*, 397(15), 2019.
- [39] T. Xiong and J. Qiu. A hierarchical uniformly high order DG-IMEX scheme for the 1D BGK equation. *J. Comput. Phy.*, 336:164–191, 2017.